Neuron

Article

Distinct prefrontal projection activity and transcriptional state conversely orchestrate social competition and hierarchy

Graphical abstract

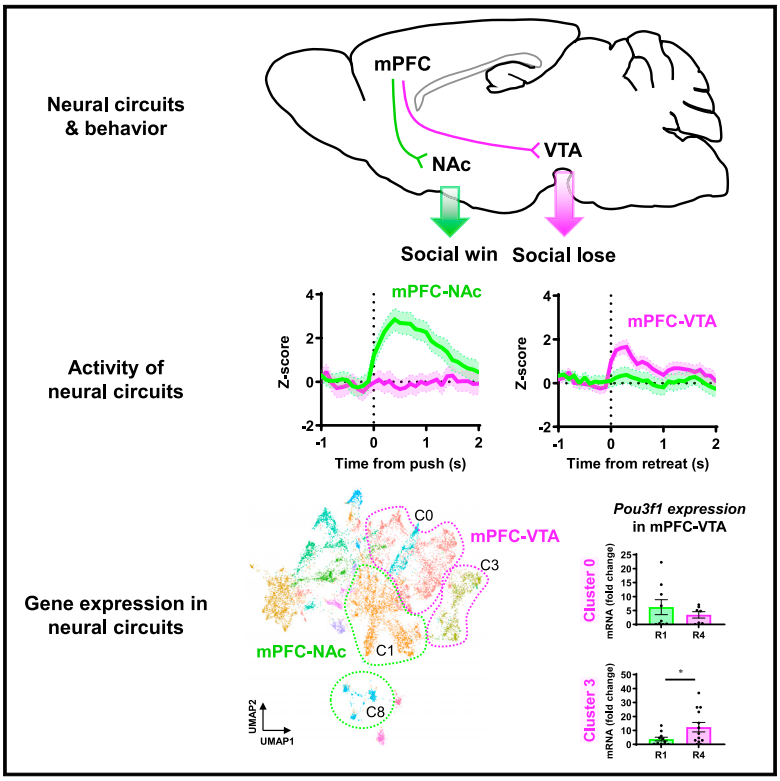

Highlights

- Distinct mPFC neural populations oppositely regulate social competition behaviors
- mPFC-NAc projection drives social winning
- mPFC-VTA projection drives social losing
- *Pou3f1* expression level in mPFC-VTA neurons control social hierarchy

Authors

Tae-Yong Choi, Hyoungseok Jeon, Sejin Jeong, ..., Byungsoo Kang, Murim Choi, Ja Wook Koo

Correspondence

murimchoi@snu.ac.kr (M.C.), jawook.koo@kbri.re.kr (J.W.K.)

In brief

Choi et al. find that distinct neuronal populations in the medial prefrontal cortex (mPFC) oppositely drive social hierarchy: mPFC neurons projecting to the nucleus accumbens (mPFC-NAc) for winning and those projecting to the ventral tegmental area (mPFC-VTA) for losing. *Pou3f1* expression level in mPFC-VTA neurons regulates social hierarchy.

Choi et al., 2024, Neuron *112*, 1–17
February 21, 2024
https://doi.org/10.1016/j.neuron.2023.11.012

CellPress

Neuron

CellPress

Article

Distinct prefrontal projection activity and transcriptional state conversely orchestrate social competition and hierarchy

Tae-Yong Choi,[1,8] Hyoungseok Jeon,[2,8] Sejin Jeong,[1,3] Eum Ji Kim,[1] Jeongseop Kim,[1,4] Yun Ha Jeong,[5] Byungsoo Kang,[6,7] Murim Choi,[2,*] and Ja Wook Koo[1,4,9,*]

[1]Emotion, Cognition and Behavior Research Group, Korea Brain Research Institute, Daegu 41062, Republic of Korea
[2]Department of Biomedical Sciences, Seoul National University College of Medicine, Seoul 03080, Republic of Korea
[3]Department of Life Sciences, Yeungnam University, Gyeongsan 38541, Republic of Korea
[4]Department of Brain Sciences, Daegu Gyeongbuk Institute of Science and Technology, Daegu 41988, Republic of Korea
[5]Neurodegenerative Disease Research Group, Korea Brain Research Institute, Daegu 41062, Republic of Korea
[6]Sysoft R&D Center, Daegu 41065, Republic of Korea
[7]Neurovascular Unit Research Group, Korea Brain Research Institute, Daegu 41062, Republic of Korea
[8]These authors contributed equally
[9]Lead contact
*Correspondence: murimchoi@snu.ac.kr (M.C.), jawook.koo@kbri.re.kr (J.W.K.)
https://doi.org/10.1016/j.neuron.2023.11.012

SUMMARY

Social animals compete for limited resources, resulting in a social hierarchy. Although different neuronal subpopulations in the medial prefrontal cortex (mPFC), which has been mechanistically implicated in social dominance behavior, encode distinct social competition behaviors, their identities and associated molecular underpinnings have not yet been identified. In this study, we found that mPFC neurons projecting to the nucleus accumbens (mPFC-NAc) encode social winning behavior, whereas mPFC neurons projecting to the ventral tegmental area (mPFC-VTA) encode social losing behavior. High-throughput single-cell transcriptomic analysis and projection-specific genetic manipulation revealed that the expression level of POU domain, class 3, transcription factor 1 (*Pou3f1*) in mPFC-VTA neurons controls social hierarchy. Optogenetic activation of mPFC-VTA neurons increases *Pou3f1* expression and lowers social rank. Together, these data demonstrate that discrete activity and gene expression in separate mPFC projections oppositely orchestrate social competition and hierarchy.

INTRODUCTION

Many social animals compete for limited resources such as food and territory, resulting in a social hierarchy within a group. An individual's social rank determines the behaviors that are appropriate for that position.[1–8] For instance, social subordinates avoid competing with social dominants to prevent physical harm and energy loss, whereas social dominants engage in agonistic interactions to obtain easy access to food and sexual partners. Therefore, social-status-specific behavioral adaptations are advantageous for individuals' health and survival in an evolutionary context.[9–12]

The medial prefrontal cortex (mPFC) is an important hub region of social competition and hierarchy.[13–17] The mPFC neurons are activated by effortful behaviors intended for winning, such as push and retreat during the social dominance tube test.[18] Modifying the synaptic efficacy or neuronal activity in the mPFC regulates social dominance.[18–21] Recent studies have revealed that social losing (i.e., retreat) and winning behaviors during the tube test activate distinct mPFC neuronal subpopulations, suggesting that they separately encode opposite aspects of social competition and hierarchy.[22,23]

Although mPFC neurons send their axonal projections to various brain regions, hypothalamic neural pathways from the mPFC have previously been reported to be associated with social competition behaviors.[19,24] Evidence shows that the mPFC neuronal subpopulations that give projections to different hypothalamic regions separately involve distinct aspects of agnostic behaviors.[24] These data support the idea that the mPFC controls specific behavioral features of social competition at the circuit level. Moreover, the mPFC neuronal subpopulations defined by connectivity have projection-specific molecular features.[25–28] Together, these results suggest that the mPFC may orchestrate social competition behaviors by manipulating gene expression and neuronal activity at the circuit level. Although molecular candidates in the mPFC that are involved in social dominance have been identified at the brain-region level,[29,30] the genes differentially expressed

Please cite this article in press as: Choi et al., Distinct prefrontal projection activity and transcriptional state conversely orchestrate social competition and hierarchy, Neuron (2023), https://doi.org/10.1016/j.neuron.2023.11.012

according to social status and their functions at the level of mPFC circuits remain unclear.

To address these questions, we identified differently activated mPFC projections in winner and loser mice using the tube test. We found that mPFC neurons projecting to the nucleus accumbens (mPFC-NAc) or ventral tegmental area (mPFC-VTA), which were previously reported to play an opposite role in social competition,[31–34] were activated in winners or losers, respectively. These observations were validated by measuring and manipulating the activities of these two mPFC projections during social competition. Single-cell RNA sequencing (scRNA-seq) of the mPFC from social dominants and subordinates was performed to investigate the projection-specific transcriptome of the mPFC-NAc or mPFC-VTA neurons. The subsequent projection-specific validation and genetic manipulation revealed that POU domain, class 3, transcription factor 1 (*Pou3f1*) in mPFC-VTA neurons was identified as a crucial factor in social hierarchy determination. Taken together, these results reveal that different neural circuit activities and gene expression in separate mPFC projections conversely control social competition and hierarchy.

RESULTS

Social competition activates the mPFC-NAc or mPFC-VTA in the winner or loser, respectively

To investigate which mPFC projections are activated in social winners or losers in the tube test, we traced activated mPFC neurons and their projections using a targeted recombination in active population under Fos promoter (FosTRAP) strategy.[35–38] We injected AAV1-phSyn1-FLEX-tdTomato-T2A-SypEGFP-WPRE into the mPFC of *Fos*^{CreER} mice to label activated neurons with tdTomato and activated axon terminals with synaptophysin-fused EGFP (SypEGFP) (Figures 1A and 1B).[39] The resultant numbers of activated mPFC neurons in winners and losers were not different, but both were higher than those in the control group (Figures 1C and 1D). However, the NAc of the winner and the VTA of the loser received more activated mPFC projections (Figures 1C and 1E). Other brain areas, such as the lateral hypothalamus (LH), mediodorsal thalamus (MDT), basolateral amygdala (BLA), and periaqueductal gray (PAG), received similar amounts of activated mPFC projections from winners and losers (Figures S1A–S1C). To clarify whether mPFC-NAc or mPFC-VTA projection was selectively activated in winners or losers, we conducted tracing retrogradely the activated cell ensemble (TRACE) experiments.[40] Two viral vectors that express Cre-inducible EYFP and mCherry retrogradely using rAAV2-retro serotype (AAVrg)[41] were injected into the NAc and VTA of *Fos*^{CreER} mice, respectively (Figure 1F). The animals were subjected to the tube test and subsequently administered 4-hydroxytamoxifen (4-OHT) 2 h after the test. Consequently, EYFP-expressing (i.e., NAc-projecting) and mCherry-expressing (i.e., VTA-projecting) mPFC neurons increased in winners and losers, respectively (Figures 1G and 1H). These results indicate that the mPFC-NAc projection is activated by social winning, whereas the mPFC-VTA projection is activated by social losing.

Next, we tested whether these two mPFC projections were differentially activated in social dominants (rank 1 [R1]) or subordinates (rank 4 [R4]) after acquiring stable social ranks. Neuronal activity measured by c-Fos expression (Figures S1D–S1I) or intrinsic excitability (Figures S2A, S2B, S2H, and S2I) did not differ between R1 and R4 in either mPFC projection. c-Fos expression in the mPFC was similar between R1 and R4 (Figure S1G). Moreover, intrinsic electrophysiological properties, such as rheobase current (Figures S2C, S2D, S2J, and S2K), membrane capacitance (C_m) (Figures S2E and S2L), resting input resistance (R_{In}) (Figures S2F and S2M), and resting membrane potential (Figures S2G and S2N) did not differ between R1 and R4 in both mPFC projections. These results suggest that the activity of mPFC-NAc or mPFC-VTA circuitry is not involved in social dominance after social rank is formed. Furthermore, the structural connectivity of the mPFC-NAc or mPFC-VTA projection between social dominants and subordinates was not different (Figures S1H and S1I). It means that the differences in mPFC-NAc or mPFC-VTA circuit activity, but not anatomical changes, affect social competition.

mPFC-NAc or mPFC-VTA projection was activated during social winning or losing behaviors, respectively

To elucidate when and how the mPFC-NAc or mPFC-VTA projection was activated during social competition, we measured the activity of these two mPFC projections during the tube test using fiber photometry (Figure 2A). AAV9-hSyn1-axon-GcaMP6s-P2A-mRuby3[42] was injected into the mPFC and fiber optic cannulas were implanted both into the NAc and VTA (Figure 2B). Fiber photometry recordings were then conducted during a tube test with multiple pairs of mice. As a result, the mPFC-NAc, but not mPFC-VTA, projection was activated when a mouse pushed (Figures 2C–2F) or approached opponents (Figures 2K–2N) and when a mouse resisted an opponent's pushes (Figures 2G–2J). In contrast, the activity of the mPFC-VTA, but not the mPFC-NAc, projection increased when an animal retreated during the tube test (Figures 2O–2R). These results suggest that the mPFC-NAc projection encodes active behaviors to win (i.e., push and approach) or to not lose (i.e., resistance) and that social losing behavior, such as retreat, is encoded in mPFC-VTA neurons.

Retreat behavior is classified into two types based on its spontaneity: active retreat, which is a retreat behavior without the opponent's pushes or approaches, and passive retreat, which is a retreat behavior triggered by an opponent's pushes. Similar to a previous study,[43] we observed more active retreats (46/81 trials, Figures S3A and S3B) than passive retreats (35/81 trials, Figures S3E and S3F). We then investigated whether active or passive retreat had a distinct effect on the activity of these two mPFC projections. Neither active nor passive retreats altered the activity of mPFC-NAc projection (Figures S3A, S3C, S3D, S3E, S3G, and S3H). However, both active and passive retreats increased the activity of mPFC-VTA projections (Figures S3B, S3C, S3D, and S3F–S3H). These findings demonstrate that all retreat behaviors, regardless of spontaneity, increase the activity of the mPFC-VTA projection.

Next, we examined whether there were differences in neural circuit activity between winners and losers. Our results revealed that the activity of the mPFC-NAc projection was higher in winners during resistance (Figures S3M and S3N) and approach

Please cite this article in press as: Choi et al., Distinct prefrontal projection activity and transcriptional state conversely orchestrate social competition and hierarchy, Neuron (2023), https://doi.org/10.1016/j.neuron.2023.11.012

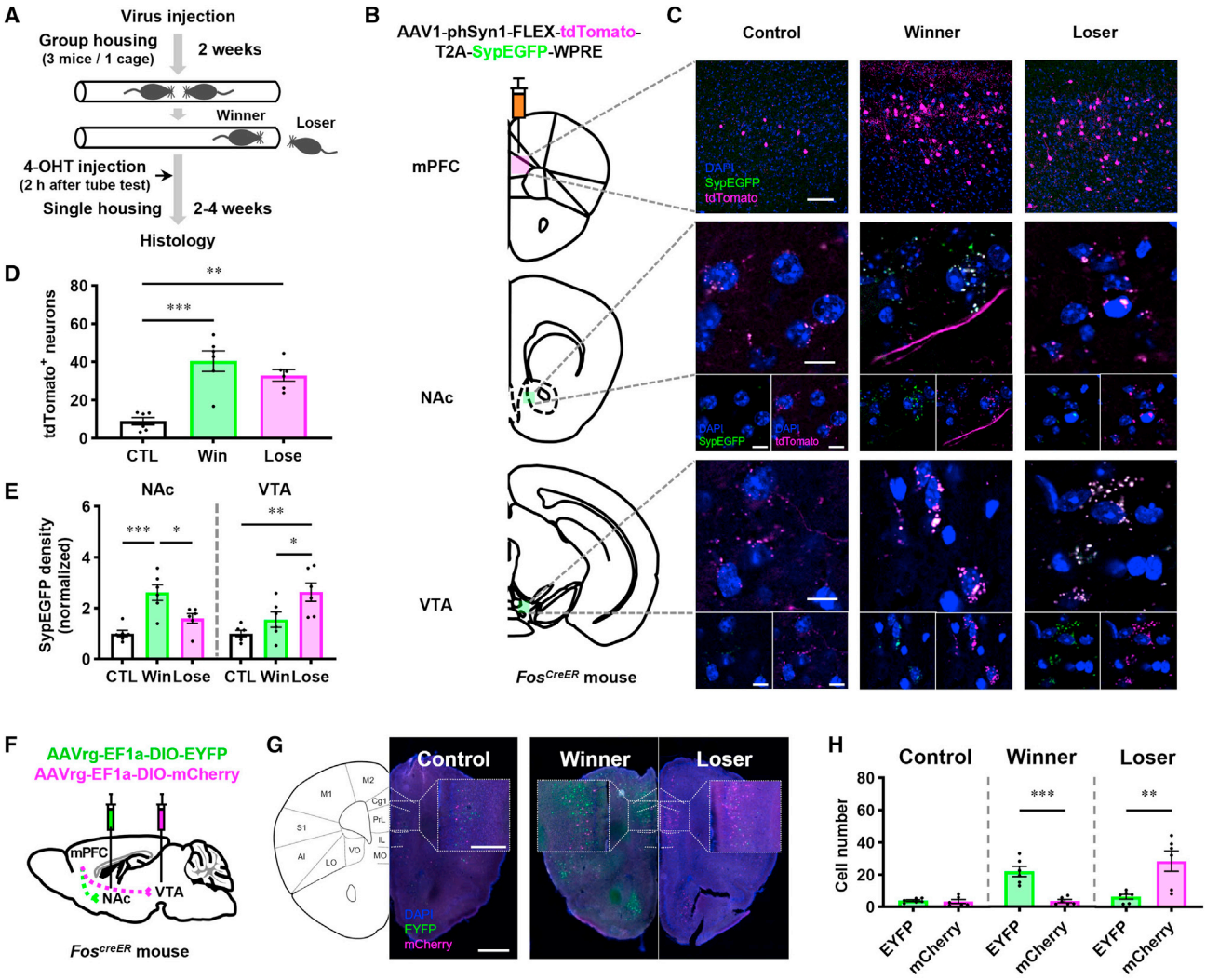

Figure 1. Social competition activates mPFC-NAc in winners and mPFC-VTA in losers

(A) Schematic illustration of the tube test for FosTRAP.

(B) Schematic illustration of viral injection for tracing activated mPFC neurons and their projections.

(C) Representative images containing activated neurons in the mPFC (top) and their projections in the NAc (middle) and VTA (bottom) by the tube test. Small images under images of the NAc or VTA show DAPI and SypEGFP (left) and DAPI and tdTomato (right). Scale bars, 0.1 mm (top); 10 μm (magnified images in middle and bottom).

(D) Quantification of tdTomato-expressing FosTRAPed neurons in the mPFC. Values are mean ± SEM (n = 6 mice per group; one-way ANOVA with Tukey's test; $^{**}p < 0.01$, $^{***}p < 0.001$).

(E) Quantification of SypEGFP-expressing activated projections. Values are mean ± SEM (n = 6 mice per group; one-way ANOVA with Tukey's test; $^{*}p < 0.05$, $^{**}p < 0.01$, $^{***}p < 0.001$).

(F) Schematic illustration of viral injection for TRACE experiments.

(G) Representative images containing the mPFC from control, winner, or loser mice, and magnified image of the area indicated by a white dashed box. Left illustration shows the coronal view of the mPFC. Scale bars, 1.0 mm; 0.5 mm (magnified images).

(H) Quantification of $EYFP^{+}$ (or mPFc-NAc) or $mCherry^{+}$ (or mPFC-VTA) neurons in the mPFC from control, winner, or loser. Values are mean ± SEM (n = 6 mice per group; Student's t test [unpaired, two-tailed]; $^{**}p < 0.01$, $^{***}p < 0.001$).

(Figures S3Q and S3R). However, there was no difference in mPFC-NAc activity during the push between winners and losers (Figures S3I and S3J). Furthermore, we observed that the activity of the mPFC-VTA projection was higher in the loser during retreat (Figures S3W and S3X), specifically in the cases of active retreat (Figures S3Wa and Xa) but not passive retreat (Figures S3Wb and S3Xb). However, mPFC-VTA activity during the push (Figures S3K and S3L), resistance (Figures S3O and S3P), and approach (Figures S3S and S3T) did not differ between winners and losers. These results suggest that there are differences in the neural circuit activity that trigger specific social competition behaviors based on social status.

Please cite this article in press as: Choi et al., Distinct prefrontal projection activity and transcriptional state conversely orchestrate social competition and hierarchy, Neuron (2023), https://doi.org/10.1016/j.neuron.2023.11.012

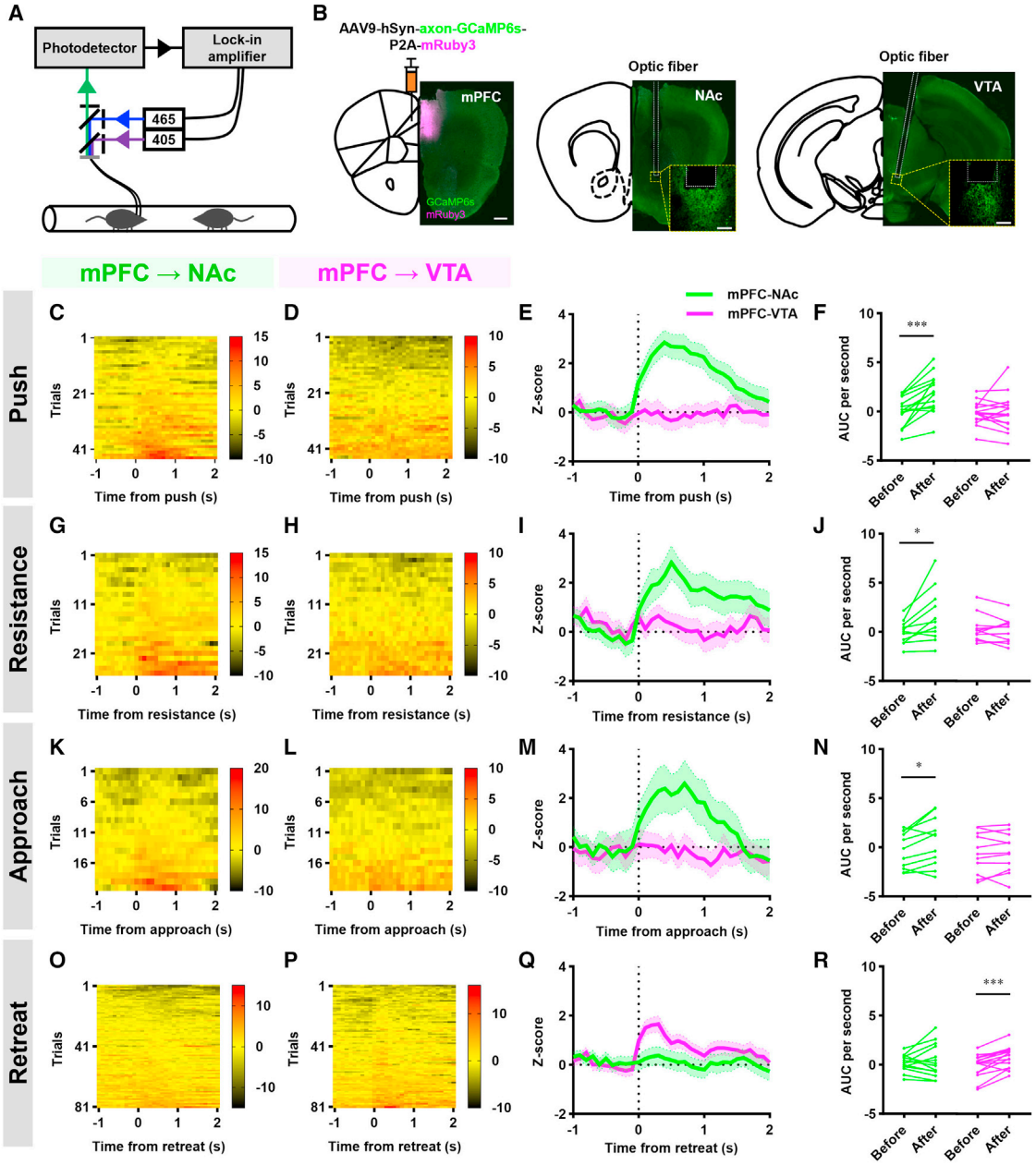

Figure 2. Different social competition behaviors are separately encoded in mPFC-NAc or mPFC-VTA projections

(A) Schematic illustration of fiber photometry during the tube test.

(B) Schematic illustrations (left) and representative images (right) of viral injection in the mPFC and optic fiber implantation in the NAc and VTA. Inset images showing magnified yellow boxed area to illustrate the area near the tip of implanted optic fiber. Scale bars, 500 μm; 200 μm (inset).

(C–F) Heatmap (C and D), peri-event plot (E), and quantification of the area under curve (AUC) per second of *Z* scored mPFC-NAc or mPFC-VTA activity aligned to the onset of pushes (F). Shading in (E) means the standard error of the mean (SEM) (n = 15 mice per group; Student's t test [paired, two-tailed]; ***$p < 0.001$).

(G–J) Heatmap (G and H), peri-event plot (I), and quantification of AUC per second of *Z* scored mPFC-NAc or mPFC-VTA activity aligned to the onset of resistances (J). Shading in (I) means SEM (n = 11 mice per group; Student's t test [paired, two-tailed]; *$p < 0.05$).

(K–N) Heatmap (K and L), peri-event plot (M), and quantification of AUC per second of *Z* scored mPFC-NAc or mPFC-VTA activity aligned to the onset of approaches (N). Shading in (M) means SEM (n = 11 mice per group; Student's t test [paired, two-tailed]; *$p < 0.05$).

(O–R) Heatmap (O and P), peri-event plot (Q), and quantification of AUC per second of *Z* scored mPFC-NAc or mPFC-VTA activity aligned to the onset of retreats (R). Shading in (Q) means SEM (n = 14 mice per group; Student's t test [paired, two-tailed]; ***$p < 0.001$).

Manipulating the mPFC-NAc or mPFC-VTA activity conversely modulates social competition and hierarchy

Next, we investigated whether manipulating the activity of either the mPFC-NAc or mPFC-VTA projection would regulate social competition behaviors in an opposing manner. To examine the behavioral effects of mPFC-NAc or mPFC-VTA inhibition, a tube test was performed on multiple pairs of mice, each with a control and a cagemate mouse that had received viral vectors that were able to genetically ablate each projection-specific neuronal subpopulation: AAVrg-mCherry-IRES-Cre into the NAc or VTA to retrogradely express Cre recombinase and AAV2-Flex-taCasp3-TEVp into the mPFC to induce Cre-dependent apoptosis (Figures 3A, 3B, 3E, and 3F).[44] This approach resulted in the ablation of over 60% of the retrogradely labeled neurons from the NAc or VTA (Figures S4A and S4D). The tube test results showed that mice with ablating mPFC-NAc projection were significantly more prone to lose (Figure 3C) and exhibited fewer pushes and more retreats during the tube test (Figure 3D). Conversely, mice with inhibited mPFC-VTA projection displayed significantly more wins (Figure 3G), with a decrease in retreats and an increase in pushes (Figure 3H). We also performed a direct social interaction test and found no difference in the social interaction time between the control and circuit-inhibited mice (Figures S4C and S4F). These results suggest that the mPFC-NAc and mPFC-VTA circuitries conversely regulate social competition, which is not associated with sociability.

We found that more mPFC-NAc or mPFC-VTA projection was activated in social winners or losers, respectively (Figure 1), and irreversible ablation of these two projections had opposite effects on social dominance behaviors (Figures 2A–2H). However, there may be slight differences between FosTRAPed neuronal populations and those ablated using a combination of retrograde expression of Cre recombinase and Cre-dependent genetic ablation. To address this, we examined the anatomical and functional similarities between mPFC neurons and their projections activated by social competition and retrogradely labeled mPFC-NAc or mPFC-VTA neurons. We injected AAV5-cFos-ER^{T2}-Cre-ER^{T2} into the mPFC of *Ai6* mice to label activated mPFC neurons during social competition (Figure S4G).[38] The same animal also received AAVrg-CAG-tdTomato into the NAc and Alexa Fluor 647-conjugated cholera toxin subunit B (CTB-647) into the VTA to retrogradely label mPFC-NAc and mPFC-VTA neurons with different fluorophores (Figures S4G–S4I). After the tube test, we observed more activated mPFC neurons expressing ZsGreen fluorescent protein in both winners and losers than in control mice (Figures S4J and S4K), as shown in Figure 1D. Additionally, the proportion of activated populations among retrogradely labeled NAc- or VTA-projecting mPFC neurons was higher in winners or in losers, respectively (Figures S4N and S4O), consistent with our observation in Figures 1F–1H. This suggests that more mPFC-NAc neurons are activated in winners, while more mPFC-VTA neurons are activated in losers during social competition. Next, we investigated whether each activated mPFC projection from the prior tube test regulated social competition behavior. We injected AAV5-cFos-ER^{T2}-Cre-ER^{T2} and AAV5-EF1a-DIO-eNpHR3.0-EYFP into the mPFC to express the inhibitory optogenetic protein only in activated neurons by prior social competition and we implanted fiber optic cannulas into the NAc or VTA to inhibit NpHR-expressing projections (Figures S4P and S4V). We performed a tube test with several pairs of mice to determine winners or losers, followed by an intraperitoneal injection of 4-OHT 2 h after the test to induce FosTRAP (Figure S4Q). After 4 weeks, we conducted another tube test with optogenetic inhibition of each projection. The results showed that optogenetic inhibition of activated mPFC-NAc projection in winners significantly decreased their social rank and winning behavior such as push (Figures S4R–S4U). In contrast, optogenetic inhibition of activated mPFC-VTA projection in losers increased their wins and decreased losing behaviors such as resistances (Figures S4W–S4Z). These results suggest that activated and retrogradely labeled mPFC-NAc or mPFC-VTA projection plays a similar role in social competition behavior.

We then tested whether the activation of mPFC-NAc or mPFC-VTA projection changes social competition and hierarchy. A viral vector was administered to four cagemates to express channelrhodopsin proteins (hChR2) in the mPFC, and a fiber optic cannula was implanted into the NAc or VTA to deliver light stimulation (Figures 3I, 3J, 3O, and 3P). After confirming stable social ranks, which were defined as the same ranking in the tube test for several consecutive days,[18,21] blue laser light was delivered to the mPFC-NAc or mPFC-VTA projection during the next tube test. The consequent photoactivation of the mPFC-NAc projection in social subordinates increased their social rank (Figures 3K–3M and S5A–S5C). The activation of the mPFC-NAc projection specifically increased the number of pushes and resistances, while decreasing the number of retreats (Figure 3N). In contrast, the photoactivation of mPFC-VTA projection in social dominants decreased their social rank (Figures 3Q–3S and S5D–S5F). Furthermore, the activation of the mPFC-VTA projection significantly increased the number of retreats (Figure 3T). However, optogenetic activation of these two projections did not alter locomotion (Figures S5H–S5L). Furthermore, social competition behaviors, such as push and retreat, were not affected by the optogenetic activation of mPFC-NAc or mPFC-VTA projection during tube tests conducted with an object instead of an animal (Figures S5M–S5S). Together, these results imply that the mPFC-NAc or mPFC-VTA projections conversely regulate social competition and hierarchy without affecting other behaviors.

Single-cell transcriptomic analysis reveals projection-specific molecular candidates for social hierarchy

To investigate the projection-specific molecular determinants in the mPFC-NAc or mPFC-VTA neurons participating in social hierarchy, we conducted scRNA-seq of the mPFC of social dominants (R1) and subordinates (R4). The mPFC tissue punches were collected and dissected, and the resulting cells were subjected to a 10× Genomics scRNA-seq pipeline (Figure 4A). After excluding low-quality and doublet cells, the resulting 41,409 cells (15,272 cells from R1 and 26,137 from R4) were clustered and analyzed (Figure S6A; Tables S1 and S2). Of these, 14,883 cells (5,325 cells from R1 and 9,558 from R4) were classified as neurons (Figures 4B and S6B) and were analyzed separately. Subsequently, we identified mPFC-NAc and mPFC-VTA neurons using previously reported projection-specific marker genes.[26] A principal component analysis plot showed a separate expression pattern of mPFC-NAc or

Please cite this article in press as: Choi et al., Distinct prefrontal projection activity and transcriptional state conversely orchestrate social competition and hierarchy, Neuron (2023), https://doi.org/10.1016/j.neuron.2023.11.012

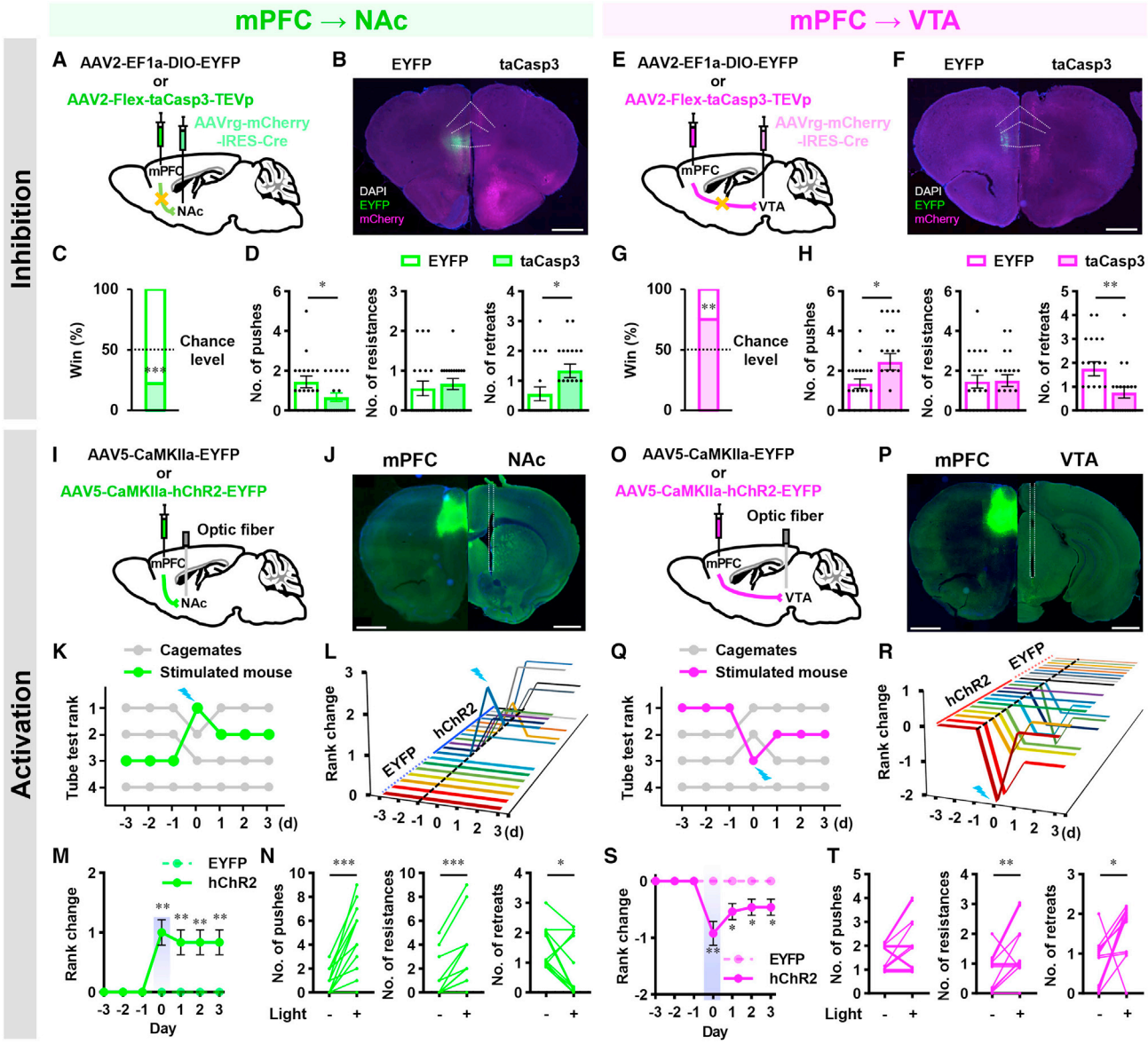

Figure 3. Manipulation of mPFc-NAc or mPFC-VTA activity oppositely modulates social competition and hierarchy

(A and E) Schematic illustration of genetic strategy to ablate mPFC-NAc (A) or mPFC-VTA (E) projection.

(B and F) Representative images of control (left) or genetic ablation (right) in mPFC-NAc (B) or in mPFC-VTA (F) projection. Scale bars, 1 mm.

(C and G) Genetic ablation of mPFC-NAc projection decreases (C), but mPFC-VTA projection increases (G) social dominance; n = 18 (C) and 20 (G) pairs; chi-squared test (two-sided); $^{**}p < 0.01$, $^{***}p < 0.001$.

(D and H) Behavioral performance of the control and mPFC-NAc-inhibited (D) or mPFC-VTA-inhibited (H) mice. Values are mean ± SEM; n = 18 (D) and 20 (H) pairs; Mann-Whitney U test (two-tailed); $^{*}p < 0.05$, $^{**}p < 0.01$.

(I and O) Schematic illustration of optogenetic activation of mPFC-NAc (I) or mPFC-VTA (O) projection.

(J and P) Representative images of the expression of hChR2 in mPFC (left) and optic fiber implantation in the NAc (J, right) or VTA (P, right) projections. Scale bars, 1 mm.

(K and Q) Results of daily tube test conducted on a cage of four mice before and after acute photostimulation of mPFC-NAc projection of the rank 3 mouse (K) or mPFC-VTA projection of the rank 1 mouse (Q) on day 0.

(L and R) Rank change following optogenetic stimulation of mPFC-NAc (L) or mPFC-VTA (R) projection in the tube test. One animal is shown on each line. On day 0, photostimulation was applied during the tube test.

(M and S) Optogenetic activation of mPFC-NAc projection increases social ranks (M), but optogenetic activation of mPFC-VTA projection decreases social ranks (S). Values are mean ± SEM; n = 7 mice (M, EYFP), 12 (M, hChR2), 8 (S, EYFP), and 13 (S, hChR2); Mann-Whitney U test (two-tailed); $^{*}p < 0.05$, $^{**}p < 0.01$.

(N and T) Behavioral performance of the same hChR2-expressing mice in mPFC-NAc (N) and mPFC-VTA (T) projections, before and after photoactivation; n = 12 (N) and 13 (T) mice; Student's t test (paired, two-tailed); $^{*}p < 0.05$, $^{**}p < 0.01$, $^{***}p < 0.001$.

Please cite this article in press as: Choi et al., Distinct prefrontal projection activity and transcriptional state conversely orchestrate social competition and hierarchy, Neuron (2023), https://doi.org/10.1016/j.neuron.2023.11.012

CellPress

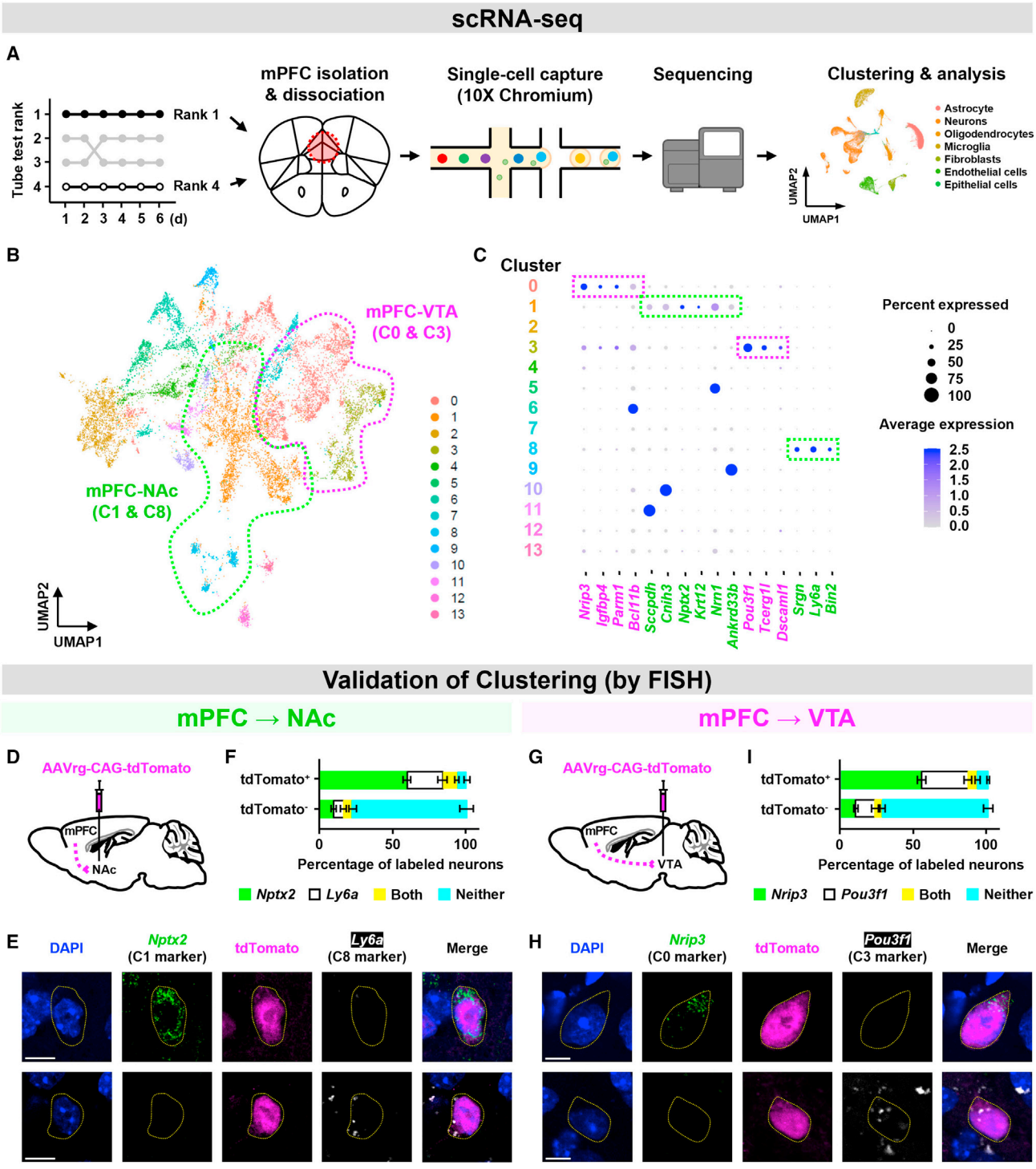

Figure 4. mPFC neurons can be clustered into mPFC-NAc or mPFC-VTA neurons using single-cell transcriptomic analysis

(A) Schematic illustration of scRNA-seq of the mPFC from R1 and R4 mice.

(B) A uniform manifold approximation and projection (UMAP) plot of 5,325 and 9,558 neurons from the mPFC of R1 and R4 mice, respectively (n = 11 mice per group).

(C) Expression of the projection-specific marker genes reported by Kim et al.[26] across identified clusters, with the colors of the clusters the same as in the UMAP in (B). mPFC-NAc neurons, C1 and C8; mPFC-VTA neurons, C0 and C3.

(D and G) Schematic illustration of viral injection in the NAc (D) or VTA (G) for FISH.

(legend continued on next page)

Please cite this article in press as: Choi et al., Distinct prefrontal projection activity and transcriptional state conversely orchestrate social competition and hierarchy, Neuron (2023), https://doi.org/10.1016/j.neuron.2023.11.012

mPFC-VTA projection-specific marker genes (Figures S6C–S6E). To verify whether projection-specific marker genes are highly expressed in each mPFC-projecting neuron, we performed the single-cell reverse transcription quantitative polymerase chain reaction (scRT-qPCR) for some projection-specific marker genes in aspirated intracellular contents of retrogradely labeled mPFC-NAc or mPFC-VTA neurons (Figure S6G). Expression levels of *Fos* and *Nrn1*, marker genes of mPFC-NAc neurons, were significantly higher in mPFC-NAc neurons than in mPFC-VTA neurons (Figure S6H). Similarly, the expression of c-Fos protein was higher in mPFC-NAc neurons than in mPFC-VTA neurons (Figure S1J). Furthermore, we found that *Pou3f1* and *Nrip3*, marker genes of mPFC-VTA neurons, were more highly expressed in mPFC-VTA neurons than in mPFC-NAc neurons (Figure S6I). It suggests that mPFC-NAc and mPFC-VTA neurons have different molecular characteristics.

In the uniform manifold approximation and projection plot, we found that mPFC-NAc projection marker genes were consistently enriched in clusters 1 (C1) and C8, while mPFC-VTA projection marker genes were higher in C0 and C3 (Figures 4B, 4C, and S6F). The remaining clusters showed low overall expression of marker genes or presented ambiguous cases in which both types of markers were expressed (Figure 4C). To confirm whether C1 and C8 correspond to mPFC-NAc neurons and C0 and C3 correspond to mPFC-VTA neurons, we examined the expression of projection-specific marker genes in retrogradely labeled mPFC-NAc or mPFC-VTA neurons using scRT-qPCR and fluorescence *in situ* hybridization (FISH). In our scRT-qPCR experiments, mPFC-NAc neurons could be divided into two groups based on the expression level of C8-enriched gene *Ly6a* using K-means clustering (Figure S6J). Similarly, the expression level of C0-enriched gene *Nrip3* allowed us to distinguish two groups within mPFC-VTA neurons (Figure S6K). In our FISH experiments, we observed that C1-enriched gene *Nptx2* and C8-enriched gene *Ly6a* were highly expressed in retrogradely labeled mPFC-NAc neurons compared with non-labeled mPFC neurons (Figures 4D–4F). Additionally, mPFC-NAc neurons that expressed *Ly6a* rarely expressed C1-enriched genes and vice versa (Figures 4E and 4F). Therefore, we classified retrogradely labeled mPFC-NAc neurons expressing *Ly6a* as C8 and retrogradely labeled mPFC-NAc neurons without *Ly6a* expression as C1. Similarly, C0-enriched gene *Nrip3* and C3-enriched gene *Pou3f1* were highly expressed in retrogradely labeled mPFC-VTA neurons compared with other mPFC neurons (Figures 4G–4I). Furthermore, mPFC-VTA neurons that expressed *Pou3f1* rarely expressed C0-enriched genes and vice versa (Figures 4H and 4I). Thus, we identified retrogradely labeled mPFC-VTA neurons expressing *Pou3f1* as C3 and retrogradely labeled mPFC-VTA neurons without *Pou3f1* expression as C0.

Next, we analyzed the candidates of differentially expressed genes (DEGs) between R1 and R4 in each mPFC projection using scRNA-seq data. Our analysis revealed that *Nptx2*, *Nrn1*, *Cnih3*, and *Ankrd33b* in C1, as well as *Mpv17* in C8 of the mPFC-NAc neurons, exhibited higher expression in social subordinates than in dominants (Figure 5A). Furthermore, we observed a higher expression of *Pou3f1* in R4 than in R1 in C3, but not in C0, of mPFC-VTA neurons (Figure 5B). To validate these DEG candidates in each projection, we performed scRT-qPCR and FISH experiments for several candidate genes predicted to be differentially expressed in each mPFC projection and cluster-enriched genes. Specifically, a retrograde viral vector was injected into the NAc or VTA to label mPFC-NAc or mPFC-VTA neurons and the tube test was performed to determine the social status of the animals (Figures 5C and S7A). Our scRT-qPCR experiments revealed that the expression of *Pou3f1* mRNA in C3, as identified by the significantly lower expression of *Nrip3* (Figure S6J), but not in C0, was higher in R4 than in R1 mice (Figure 5D). Similarly, our FISH experiments demonstrated that the mRNA level of *Pou3f1* in C3, distinguished by the absence or significantly lower expression of *Nrip3* and the presence of *Pou3f1* among retrogradely labeled mPFC-VTA neurons, but not in C0, showed higher expression in R4 than in R1 mice (Figures 5E and 5F). However, the DEG candidates in mPFC-NAc neurons identified through scRNA-seq data were not validated by scRT-qPCR (Figure S7B) and FISH (Figures S7C–S7L). Together, these results suggest that the expression level of *Pou3f1* in mPFC-VTA neurons, especially in C3, may affect social hierarchy.

Although *Pou3f1* controls neurodevelopment and myelination,[45] it remains unclear how this gene in the mPFC-VTA neurons modulates the social hierarchy. Identifying the downstream genes regulated by the Pou3f1 transcription factor that binds to the octamer motif (5′-ATTTGCAT-3′) would thus be helpful.[46–49] Therefore, we re-analyzed previous chromatin immunoprecipitation sequencing (ChIP-seq) studies using Pou3f1.[49–51] Gene ontology (GO) enrichment analysis of genes near the Pou3f1 binding motifs revealed several notable terms on synaptic function (i.e., glutamatergic synapse, synaptic membrane, presynapse, etc.) as well as terms on neurodevelopment (i.e., forebrain development and positive regulation of nervous system development) (Figure S8). This suggests that *Pou3f1* expression in mPFC-VTA neurons may control social competition and hierarchy by regulating synaptic functions in the neural circuit.

Manipulating Pou3f1 expression in the mPFC-VTA regulates social hierarchy

To examine whether the expression level of *Pou3f1* in mPFC-VTA neurons regulates individuals' social status, we first suppressed

(E) Representative FISH images of mPFC-NAc neurons, which are retrogradely labeled with tdTomato and are probed for *Nptx2* transcripts and *Ly6a* transcripts. Nuclei were stained with DAPI. Scale bars, 10 μm.

(F) Quantification of *Nptx2*- or *Ly6a*-expressing mPFC-NAc (or tdTomato$^+$) or other neurons (or tdTomato$^-$) (n = 128 cells from 4 mice [*Nptx2*$^+$/tdTomato$^+$], 52, 4 [*Ly6a*$^+$/tdTomato$^+$], 21, 4 [both/tdTomato$^+$], 14, 4 [neither/tdTomato$^+$], 16, 4 [*Nptx2*$^+$/tdTomato$^-$], 12, 4 [*Ly6a*$^+$/tdTomato$^-$], 11, 4 [both/tdTomato$^-$], 134, 4 [neither/tdTomato$^-$]).

(H) Representative FISH images of mPFC-VTA neurons, which are retrogradely labeled with tdTomato and are probed for *Nrip3* transcripts and *Pou3f1* transcripts. Nuclei were stained with DAPI. Scale bars, 10 μm.

(I) Quantification of *Nrip3*- or *Pou3f1*-expressing mPFC-VTA (or tdTomato$^+$) or other neurons (or tdTomato$^-$) (n = 122 cells from 4 mice [*Nrip3*$^+$/tdTomato$^+$], 74, 4 [*Pou3f1*$^+$/tdTomato$^+$], 16, 4 [both/tdTomato$^+$], 13, 4 [neither/tdTomato$^+$], 19, 4 [*Nrip3*$^+$/tdTomato$^-$], 25, 4 [*Pou3f1*$^+$/tdTomato$^-$], 10, 4 [both/tdTomato$^-$], 194, 4 [neither/tdTomato$^-$]).

Please cite this article in press as: Choi et al., Distinct prefrontal projection activity and transcriptional state conversely orchestrate social competition and hierarchy, Neuron (2023), https://doi.org/10.1016/j.neuron.2023.11.012

CellPress

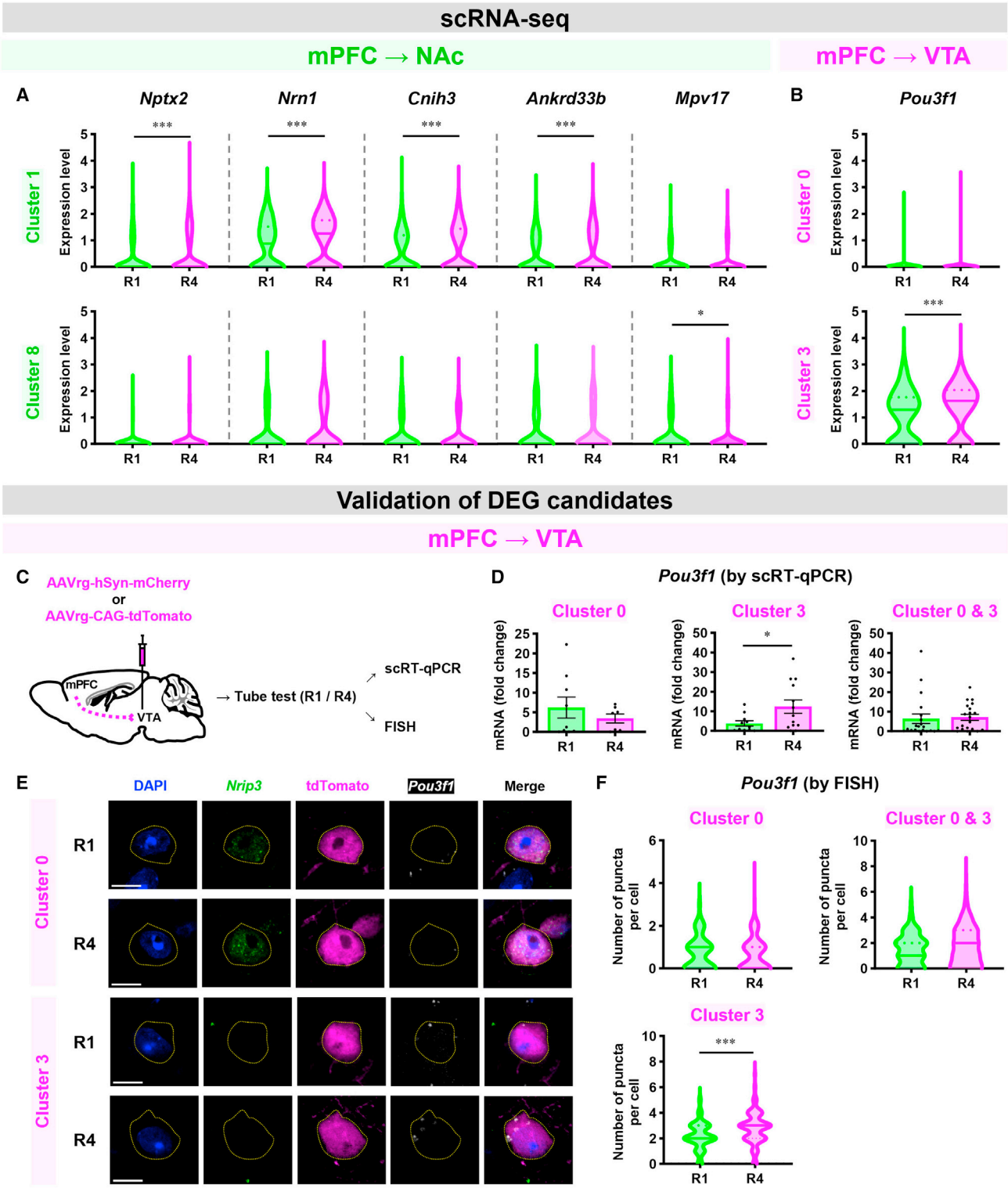

Figure 5. Social hierarchy-dependent projection-specific DEGs can be analyzed by scRNA-seq and validated by FISH

(A and B) Social hierarchy-dependent DEG candidates in mPFC-NAc (A) or mPFC-VTA (B) neurons by scRNA-seq analysis; n = 1,331 neurons (A, cluster 1, R1), n = 2,100 (A, cluster 1, R4), n = 219 (A, cluster 8, R1), n = 308 (A, cluster 8, R4), n = 1,346 (B, cluster 0, R1), n = 2,361 (B, cluster 0, R4), n = 449 (B, cluster 3, R1), and n = 675 (B, cluster 3, R4); Wilcoxon rank-sum test; *p < 0.05, ***p < 0.001.

(C) Schematic illustration of scRT-qPCR and FISH experiments to confirm social hierarchy-dependent projection-specific DEG candidates.

(legend continued on next page)

Please cite this article in press as: Choi et al., Distinct prefrontal projection activity and transcriptional state conversely orchestrate social competition and hierarchy, Neuron (2023), https://doi.org/10.1016/j.neuron.2023.11.012

the expression of *Pou3f1* in mPFC-VTA neurons in social subordinates (i.e., R3 or R4) by expressing short hairpin RNA (shRNA) against *Pou3f1* (Figures 6A, 6B, S9A, and S9B). 4 weeks after the viral injection, the social rank of the social subordinates that received *Pou3f1* shRNA in mPFC-VTA neurons increased (Figures 6C–6E, S9C, and S9D). Similarly, the knockdown of *Pou3f1* in mPFC-VTA neurons of social subordinates reduced retreats and increased pushes (Figure 6F). To test whether the winner effect of the *Pou3f1* knockdown in mPFC-VTA neurons observed in the tube test can be transferred to another social dominance behavior, we developed a behavioral test named the wet-bedding avoidance (WBA) test, which permits the investigation of individuals' territorial instincts to occupy the platform for avoiding wet bedding in a cage (Figure S9I). We found that social ranks in the WBA test, which were determined by how long each mouse occupied the platform, were well correlated with the tube test ranks (Figures S9J–SL). The total time on the platform and social ranks of the WBA test also increased after the knockdown of *Pou3f1* in mPFC-VTA neurons, similar to the tube test (Figure 6G).

Next, we tested whether the overexpression of *Pou3f1* in mPFC-VTA neurons of social dominants (R1 or R2) decreased their social ranks (Figures 6A, 6H, S9E, and S9F). The overexpression of *Pou3f1* in mPFC-VTA neurons decreased the tube test ranks (Figures 6I–K, S9G, and S9H) and the number of pushes but increased the number of retreats during the tube test (Figure 6L). Additionally, the total amount of time occupying the platform and social ranks in the WBA test were reduced by the overexpression of *Pou3f1* in mPFC-VTA neurons (Figure 6M). These results indicate that the expression level of *Pou3f1* in mPFC-VTA neurons can modulate social competition and hierarchy.

Activation of the mPFC-VTA increases Pou3f1 expression and reduces social dominance

We discovered that the optogenetic activation of mPFC-VTA projection (Figures 3O–3T) or the overexpression of *Pou3f1* in mPFC-VTA neurons (Figures 6H–6M) reduced social rank. These findings raise the question of whether mPFC-VTA activity and *Pou3f1* expression are correlated with the regulation of the social hierarchy. To address this question, we directly stimulated mPFC-VTA neurons by injecting a retrograde viral vector to express Cre recombinase (AAVrg-CAG-Cre) into the VTA, as well as Cre-inducible control or hChR2-expressing viral vectors (AAV5-EF1a-DIO-EYFP [or mCherry] or AAV5-EF1a-DIO-hChR2(H134R)-EYFP [or mCherry]) into the mPFC to determine whether *Pou3f1* expression in these neurons was altered (Figures 7A and 7B). After confirming stable tube test ranks, optogenetic stimulation was applied to the social dominants (R1 or R2) during the tube test. As shown in Figures 3O–3T, the photoactivation of mPFC-VTA neurons reduced the social rank (Figures 7C–7E, S10A, and S10B). Also, this manipulation decreased pushes and increased retreats (Figure 7F). 3 days after optogenetic stimulation, we performed scRT-qPCR or FISH experiments to determine the expression level of *Pou3f1*. As similarly observed in Figures 5C–5F, we found that *Pou3f1* expression in C3, but not in C0, was higher in social subordinates without optogenetic activation (R3/R4 + EYFP [or mCherry]) than in social dominants without optogenetic activation (R1/R2 + EYFP [or mCherry]) (Figures 7G–7I and S10C). The photoactivation of mPFC-VTA neurons not only reduced the social rank (Figures 7C–7F) but also increased the expression level of *Pou3f1* in C3 (Figures 7G–7I and S10C). We also examined the expression level of this gene immediately after photostimulation on day 0. Animals that experienced a decrease in social rank due to optogenetic activation of mPFC-VTA neurons were sacrificed 30 min after photostimulation for FISH experiments (Figure S10B). As a result, *Pou3f1* expression in C3, but not C0, of the mPFC-VTA neurons from social dominants was increased by optogenetic activation of mPFC-VTA neurons (Figures S10D and S10E). These results suggest that the activation of mPFC-VTA neurons increases the expression of *Pou3f1* in the C3-projecting subpopulation, thereby reducing the social hierarchy.

DISCUSSION

In this study, we discovered that the mPFC-NAc and mPFC-VTA projections play opposing roles in social competition and hierarchy. This provides compelling evidence that distinct neuronal populations in the mPFC encode different social competition behaviors.[18,19,21–23] Furthermore, our projection-specific transcriptomic analysis with scRNA-seq data using mPFC projection-specific marker genes[26] and subsequent genetic manipulations uncovered projection-specific molecular determinants for social dominance. Overall, these findings suggest that prefrontal functions in social dominance behaviors are distributed among highly specialized mPFC projections (e.g., mPFC-NAc vs. mPFC-VTA) that contain distinct molecular features or mechanisms for social competition and hierarchy.

Converse roles of mPFC-NAc and mPFC-VTA in social competition and hierarchy

We discovered that more mPFC-NAc or mPFC-VTA projection was activated in social winners or losers, respectively, through FosTRAP and TRACE experiments (Figures 1 and S1A–S1D). However, it remained unclear whether winning behaviors, such as push and resistance, activated the mPFC-NAc projection, while losing behavior, such as retreat, activated the mPFC-VTA projection. We directly measured neural circuit activity during the tube test using fiber photometry to pinpoint the precise timing of these activations during each social competition

(D) scRT-qPCR validation of *Pou3f1* expression in mPFC-VTA neurons between R1 and R4. All the data represented the relative fold change of *Pou3f1* mRNA expression. Values are mean ± SEM (n = 9 cells from 3 mice [cluster 0, R1], 7, 3 [cluster 0, R4], 11, 3 [cluster 3, R1], 13, 3 [cluster 3, R4], 18, 3 [clusters 0 and 3, R1], and 20, 3 [clusters 0 and 3, R4]; Student's t test [unpaired, two-tailed]; *p < 0.05).

(E) Representative FISH images of retrogradely labeled mPFC-VTA neurons with (cluster 0) or without *Nrip3* expression (cluster 3), which are probed for *Pou3f1* transcripts from R1 (top) and R4 (bottom). Nuclei were stained with DAPI. Scale bars, 10 μm.

(F) Violin plots showing number of *Pou3f1* puncta per cell for FISH in (E); n = 178 cells from 4 mice (cluster 0, R1), 197, 4 (cluster 0, R4), 200, 4 (cluster 3, R1), 196, 4 (cluster 3, R4), 378, 4 (clusters 0 and 3, R1), and 393, 4 (clusters 0 and 3, R4); Student's t test (unpaired, two-tailed); ***p < 0.001.

Please cite this article in press as: Choi et al., Distinct prefrontal projection activity and transcriptional state conversely orchestrate social competition and hierarchy, Neuron (2023), https://doi.org/10.1016/j.neuron.2023.11.012

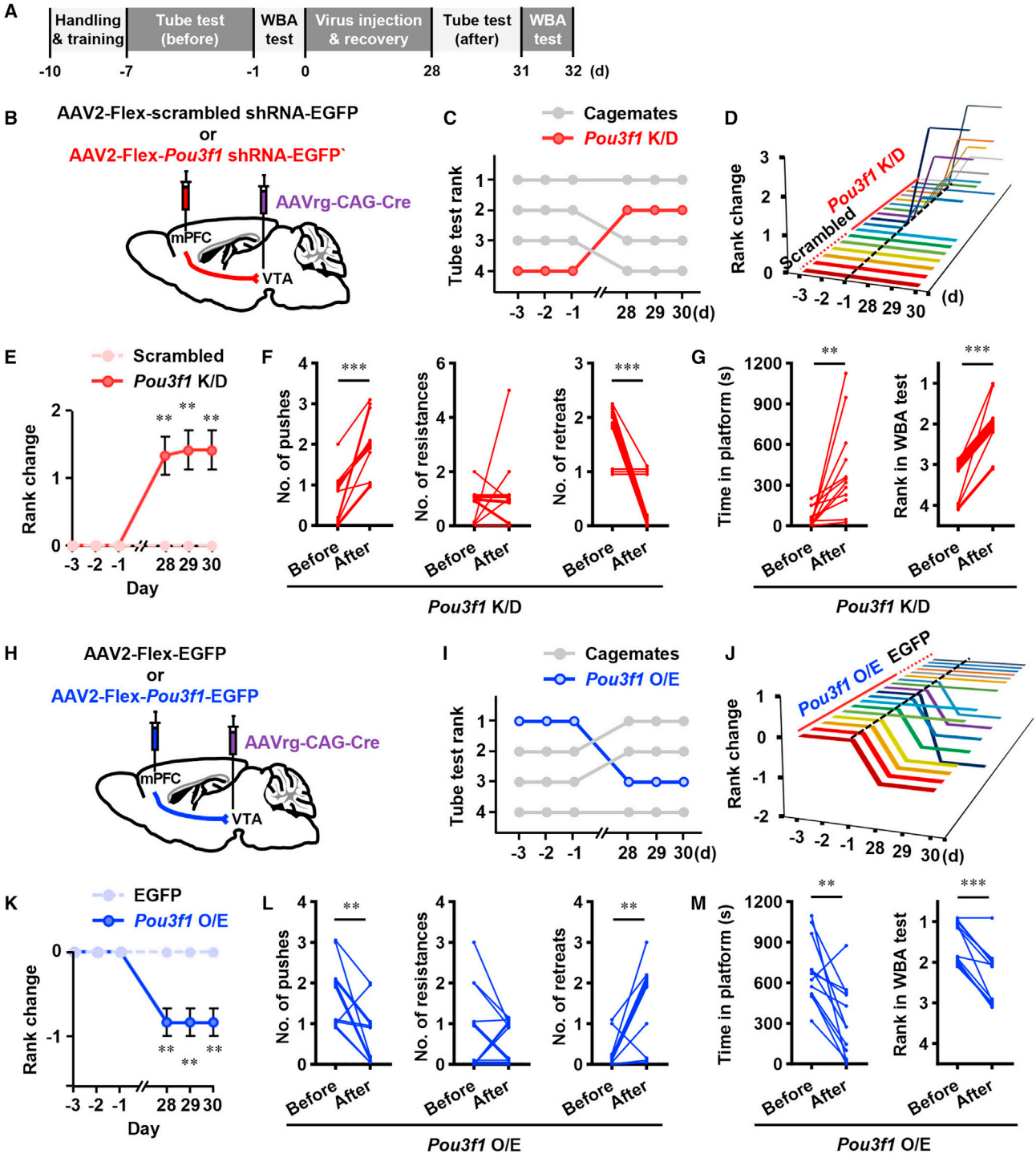

Figure 6. Manipulation of *Pou3f1* expression in mPFC-VTA neurons bidirectionally regulates social hierarchy

(A) Experimental schedule of behavioral tests for social competition and hierarchy before and after manipulating the expression of projection-specific DEGs.

(B and H) Schematic illustration of the knockdown (B, *Pou3f1* K/D) or the over-expression (H, *Pou3f1* O/E) of *Pou3f1* in mPFC-VTA neurons.

(C and I) Results of a daily tube test performed on a group of 4 mice before and after *Pou3f1* K/D in mPFC-VTA neurons of the R4 mouse (C) or *Pou3f1* O/E in mPFC-VTA neurons of the R1 mouse (I).

(D and J) Rank change following *Pou3f1* K/D in mPFC-VTA neurons of social subordinates (D) or *Pou3f1* O/E in mPFC-VTA of social dominants (J) in the tube test. One animal is shown on each line. Viral vectors were injected on day 0.

(legend continued on next page)

Please cite this article in press as: Choi et al., Distinct prefrontal projection activity and transcriptional state conversely orchestrate social competition and hierarchy, Neuron (2023), https://doi.org/10.1016/j.neuron.2023.11.012

behavior (Figures 2 and S3). The mPFC-NAc projection was activated when a mouse pushed another mouse, regardless of the opponent's behavior such as resistance or retreat (Figures 2C, 2E, and 2F). In contrast, the mPFC-VTA projection was activated when a mouse actively (Figures S3B–S3D) or passively retreated (Figures S3F–S3H) during the tube test. Based on these results, we conclude that distinct social competition behaviors are encoded separately in mPFC-NAc and mPFC-VTA projections.

In the present study, one of our main findings is that the mPFC-NAc and mPFC-VTA projections conversely control social competition and hierarchy. This raises a question regarding whether these two mPFC projections operate independently or whether one mPFC projection inhibits the other. We can rule out the possibility that the same mPFC neurons differentially control the NAc and VTA because the mPFC-NAc and mPFC-VTA neurons are located in different layers (i.e., mPFC-NAc neurons in layer 2/3–5a and mPFC-VTA neurons in layer 5b–6) and few mPFC neurons project to both the NAc and VTA (Figures S1D, S1H, S1I, S4G–S4J, S4L, and S4M).[25,26,28] We found that pushing or retreating enhanced the activity of mPFC-NAc or mPFC-VTA neurons, respectively, but had no effect on the activity of another projection (Figures 2C–2F and 2O–2R). This implies that these two projections independently participate in social competition behaviors.

Additionally, we discovered that the mPFC-NAc neurons encode social winning behaviors, such as push and resistance (Figures 2C–2J), while the mPFC-VTA neurons encode social losing behaviors, such as retreat (Figures 2O–2R). These results strongly support previous findings that one-third of push-encoding mPFC neurons are also activated when a mouse resists an opponent's pushes[18] and retreat behavior is encoded in distinct neuronal subpopulations in the mPFC.[22,23] However, a discrepancy exists between our findings and those of previous studies. Although other researchers have reported that distinct mPFC neurons encode push and approach,[22,23] our findings show that these two behaviors enhance the activity of mPFC-NAc neurons (Figures 2C–2F and 2K–2N). This may be due to the restriction of fiber photometry, which measures the activity of neuronal populations without considering cellular heterogeneity. Different mPFC-NAc neuronal subpopulations may encode a push or an approach separately.

The NAc and VTA are key components of the mesolimbic system, which controls reward and motivation by regulating dopaminergic neurotransmission from the VTA to NAc and other brain areas.[52,53] These two brain areas conversely control social hierarchy. Pharmacological lesions or inhibition of the NAc reduces the social dominance,[32,33] but pharmacological inhibition of the VTA increases the social dominance.[31,34] These results are consistent with the behavioral alterations that occur when the mPFC projections to these two brain areas are repressed (Figures 3A–3H).

Optogenetic activation of mPFC-NAc or mPFC-VTA led to an increase or decrease in social rank, respectively (Figures 3I–3T). Interestingly, the rank changes induced by these manipulations persisted for several days, even without light stimulation. This phenomenon can be attributed to modifications in neural circuit plasticity or metabolic changes induced by the optogenetic stimulation and/or alterations in social competition behaviors during the tube test. Social dominants and subordinates exhibit differences in activation level,[32] synaptic function,[33] and energy metabolism[3,32] in the NAc, and manipulating these processes can modify the social hierarchy.[32,33,54,55] These changes can potentially lead to long-term alterations in social dominance behavior.

The mPFC neurons are connected with many other brain areas and can modulate social dominance through top-down circuitries by monitoring ongoing conflicts, evaluating different behavioral options, and contributing to behavioral responses.[56–58] In addition to the mPFC-NAc and mPFC-VTA projections in our study, the LH-projecting mPFC neurons (mPFC-LH) also encode social competition behaviors.[19,24] However, the mPFC-LH projection was excluded in our study because it was not activated in either winners or losers in the tube test (Figures S1A–S1C). It suggests that different mPFC projections are involved, depending on what animals compete for: mPFC-LH neurons encode social competition for food, whereas mPFC-NAc or mPFC-VTA neurons encode social competition for territory.

Role of Pou3f1 in mPFC-VTA in social competition and hierarchy

Pou3f1, also known as *Oct6* (octamer-binding transcription factor 6), *Tst-1* (Testes-1), and *SCIP* (suppressed cyclic AMP [cAMP] inducible POU), was first identified in the embryonic neural tube and the adult brain,[59] as well as in myelin-forming glia.[47] Pou3f1 acts as a transcription factor that regulates the development of the nervous system in embryonic stem cells[45,46,48,49,59–61] and the myelination of Schwann cells and oligodendrocytes.[45,47] *Pou3f1* is also an mPFC-VTA projection marker gene that is mostly found in cortical layer 5.[26,28] In our study, *Pou3f1* was identified as an mPFC-VTA projection-specific DEG between social dominants and subordinates. Social subordinates had greater expression levels of *Pou3f1* than those of social dominants in the specific subpopulation of mPFC-VTA neurons, C3 (Figure 5). Although it is technically difficult to manipulate *Pou3f1* expression in C3, we showed that manipulating the expression level of this gene in whole mPFC-VTA neurons regulates social competition and hierarchy (Figure 6). Moreover, the expression level of *Pou3f1* in C3 was decreased by the optogenetic activation of mPFC-VTA neurons (Figure 7). These findings provide compelling evidence that the activity of mPFC-VTA neurons alters *Pou3f1* expression, which, in turn, controls social dominance.

However, how the expression level of *Pou3f1* in mPFC-VTA neurons regulates social dominance behavior remains unclear.

(E and K) *Pou3f1* K/D in mPFC-VTA neurons of social subordinates increases (E), but *Pou3f1* O/E in mPFC-VTA neurons of social dominants decreases their social ranks (K). Values are mean ± SEM; n = 6 mice (E, Scrambled), 12 (E, *Pou3f1* K/D), 6 (K, EGFP), and 12 (K, *Pou3f1* O/E); Mann-Whitney U test (two-tailed); $^{**}p < 0.01$.
(F and L) Comparison of behavioral performance of same mice before and after *Pou3f1* K/D (F) or O/E (L) in mPFC-VTA neurons (n = 12 mice per group; Student's t test [paired, two-tailed]; $^{**}p < 0.01$, $^{***}p < 0.001$).
(G and M) Changes in time on the platform (left) and rank (right) in wet bedding avoidance (WBA) test by *Pou3f1* K/D (G) or O/E (M) in mPFC-VTA neurons (n = 12 mice per group; Student's t test [paired, two-tailed]; $^{**}p < 0.01$, $^{***}p < 0.001$).

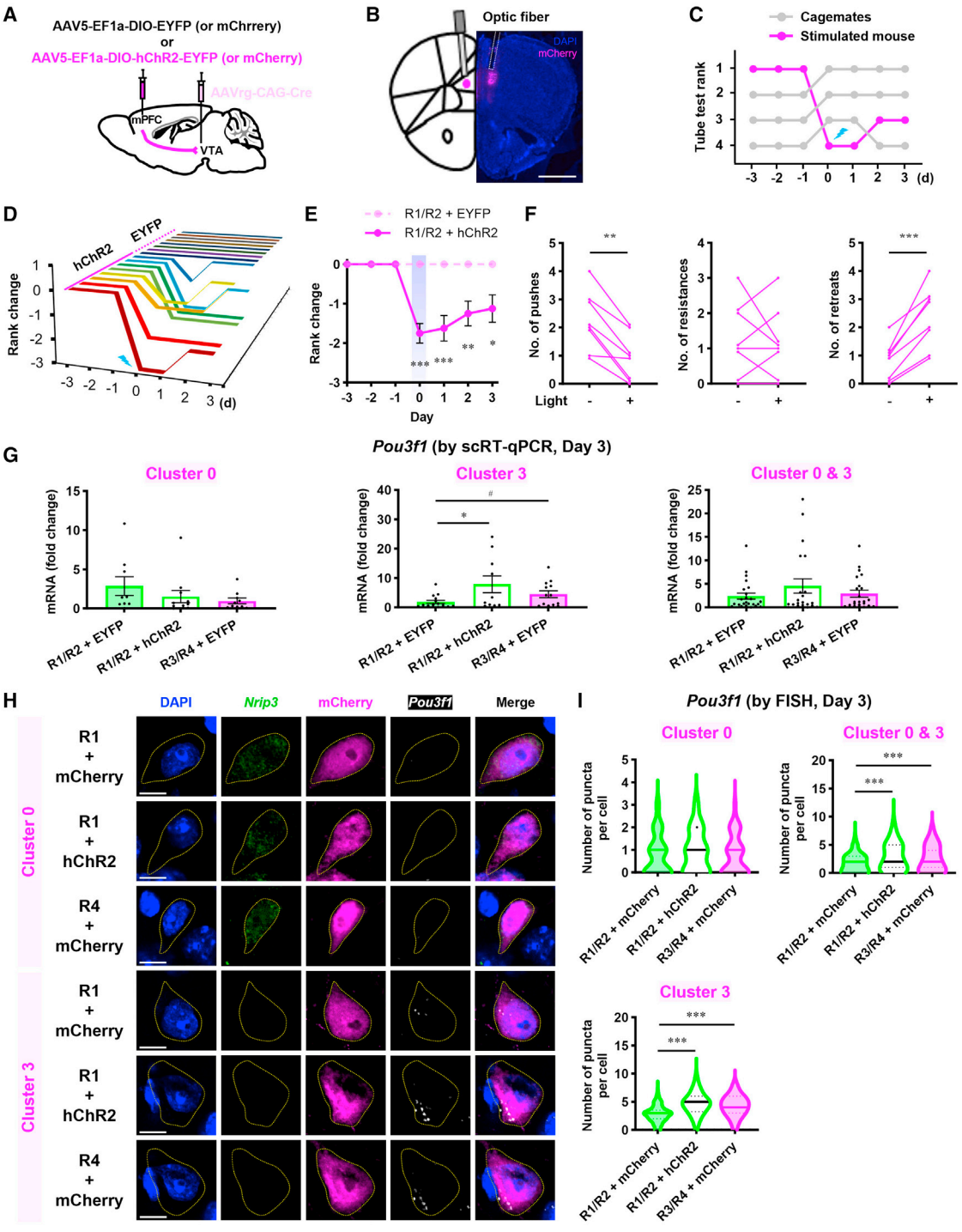

Figure 7. Optogenetic activation of mPFC-VTA neurons increases *Pou3f1* expression and decreases social ranks

(A) Schematic illustration of virus injection for optogenetic manipulation of mPFC-VTA neurons.

(B) Schematic illustration (left) and representative image (right) showing the expression of hChR2 and the implantation of the optic fiber in the mPFC.

(C) Results of a daily tube test conducted on a cage of 4 mice, before and after optogenetic activation of mPFC-VTA neurons of the R1 mouse on day 0.

(D) Rank change following optogenetic activation of mPFC-VTA neurons in the tube test. One animal is shown on each line. Photostimulation was applied during the tube test on day 0.

(E) Optogenetic activation of mPFC-VTA neurons of social dominants decreases their social ranks. Values are mean ± SEM (n = 8 mice per group; Mann-Whitney U test [two-tailed]; *p < 0.05, **p < 0.01, ***p < 0.001).

(legend continued on next page)

Please cite this article in press as: Choi et al., Distinct prefrontal projection activity and transcriptional state conversely orchestrate social competition and hierarchy, Neuron (2023), https://doi.org/10.1016/j.neuron.2023.11.012

According to recent scRNA-seq studies using mPFC tissues, *Pou3f1* is a unique marker gene for a subtype of excitatory neurons in layer 5 of the mPFC.[62–65] Our GO analysis with Pou3f1 ChIP-seq data from previous literature revealed several notable terms, such as glutamatergic synapse, synaptic membrane, and presynapse (Figure S8). These suggest that *Pou3f1* expression in mPFC-VTA neurons controls social competition and hierarchy by regulating the excitatory synaptic function of the mPFC-VTA circuitry. Furthermore, *Pou3f1* expression can be increased by intracellular cAMP, a second messenger that is enhanced by the activation of G-protein coupled receptors coupled to Gs protein (Gs-GPCRs) and adenylyl cyclase,[47] or estrogen.[66] The activation of Gs-GPCRs raises intracellular cAMP levels, which in turn increases neuronal activity, and the deletion of a gene encoding the estrogen receptor β reduces aggressive behavior.[67] It suggests that Gs-GPCR-activating neuromodulators or estrogen can regulate social hierarchy by manipulating mPFC-VTA circuit activity and *Pou3f1* expression.

Limitations of the study

Our study demonstrated that the mPFC orchestrates social competition behaviors by governing two discrete projections with opposite functions (i.e., mPFC-NAc vs. mPFC-VTA) as working units that perform specific behavioral features of social competition at the circuit level. As mentioned above, other mPFC projections may be involved in the regulation of social competition behaviors according to spontaneity (e.g., active vs. passive retreats) or reward attributes (e.g., food, territory, or mating). Additionally, social competition can be controlled by certain neuronal ensembles in the mPFC at the cell-type[21] or circuit level,[19] which requires further study.

We found that distinct social competition behaviors, such as push or retreat, activated specific mPFC populations (Figures 2 and S3). However, the time kinetics of the GCaMP signals in our results differ from those reported in previous studies.[21,23] This discrepancy is probably due to differences in experimental methods, specifically calcium imaging with single-cell resolution (e.g., miniscope) versus bulk population (e.g., fiber photometry). Another contributing factor may be the method used to determine the timestamps of specific behavioral onsets, whether automatic or manual. Further research will benefit from more refined techniques for measuring neural activity with higher temporal resolution and analyzing specific behavioral events during social competition.

The two fundamental actions during the tube test are push and retreat, which oppose each other regarding their net effects. We observed that the mPFC-NAc or mPFC-VTA circuit selectively drives push or retreat, respectively. However, manipulating these circuits also affected other aspects of social competition behaviors. For example, optogenetic activation of mPFC-NAc increased push and resistance while decreasing retreat (Figure 3N). Future experiments involving behavioral event-specific manipulation of neural circuits will be valuable for elucidating the precise neural circuit mechanisms that underlie social competition behavior.

The projection-specific molecular/physiological underpinning of social competition behaviors in the mPFC also requires further investigation. The mechanism by which the neural activity of mPFC-VTA projections modulates *Pou3f1* expression and its related molecular/physiological mechanisms in mPFC-VTA neurons and vice versa has not been studied. Regarding the mPFC-NAc projection, the expression levels of *Nptx2*, *Nrn1*, *Cnih3*, and *Ankrd33b* in the C1 and *Mpv17* in C8, which were identified as DEG candidates in our scRNA-seq analysis (Figure 5A) but were not validated by scRT-qPCR (Figure S7B) and FISH (Figures S7C–S7L), may have relevance to social hierarchy. In particular, these DEG candidates also served as marker genes for the mPFC-NAc projection, indicating that their molecular features are closely associated with the functions of this projection. Specifically, *Nptx2* (Neuronal pentraxin 2),[68,69] *Nrn1* (Neuritin 1),[70,71] and *Cnih3* (Cornishon family AMPA receptor auxiliary protein 3)[72,73] are known to be associated with synaptic function. Further investigation is required to determine whether the synaptic function within the mPFC-NAc circuit plays a role in social hierarchy behavior. Furthermore, mPFC-NAc neurons display functional heterogeneity in response to various social winning behaviors (Figures 2C–2N), implying the potential for social-hierarchy-dependent DEG candidates in mPFC-NAc neurons to play significant roles in distinct mPFC-NAc neuronal clusters that encode specific social winning behavior. A pivotal step toward a comprehensive understanding of the prefrontal functions underlying social competition behaviors would be to elucidate the behavioral/physiological implications of these projection-specific DEGs.

STAR★METHODS

Detailed methods are provided in the online version of this paper and include the following:

(F) Behavioral performance of the same hChR2-expressing mice in mPFC-VTA neurons before and after photoactivation (n = 8 mice; Student's t test [paired, two-tailed]; $^{**}p < 0.01$, $^{***}p < 0.001$).

(G) *Pou3f1* expression level in mPFC-VTA neurons from social dominants (rank 1 or 2) without or with optogenetic activation of mPFC-VTA neurons or from social subordinates (rank 3 or 4) at day 3. Values are mean ± SEM (n = 9 cells from 4 mice [cluster 0, R1/R2 + EYFP], 11, 4 [cluster 0, R1/R2 + hChR2], 10, 4 [cluster 0, R3/R4 + EYFP], 15, 4 [cluster 3, R1/R2 + EYFP], 10, 4 [cluster 3, R1/R2 + hChR2], 13, 4 [cluster 3, R3/R4 + EYFP], 24, 4 [clusters 0 and 3, R1/R2 + EYFP], 21, 4 [clusters 0 and 3, R1/R2 + hChR2], and 23, 4 [clusters 0 and 3, R3/R4 + EYFP]; one-way ANOVA with Tukey's test; $^{*}p < 0.05$ [R1/R2 + EYFP vs. R3/R4 + EYFP in cluster 3; $^{\#}p < 0.05$ by Student's t test; unpaired, two-tailed]).

(H) Representative FISH images of retrogradely labeled mPFC-VTA neurons with (cluster 0) or without *Nrip3* expression (cluster 3), which are probed for *Pou3f1* transcripts from R1 without (top) or with photostimulation (middle) or R4 without photostimulation (bottom) at day 3. Nuclei were stained with DAPI. Scale bars, 10 μm.

(I) Violin plots showing number of *Pou3f1* puncta per cell for FISH in (H) (n = 109 cells from 4 mice [cluster 0, R1/R2 + mCherry], 115, 4 [cluster 0, R1/R2 + hChR2], 113, 4 [cluster 0, R3/R4 + mCherry], 109, 4 [cluster 3, R1/R2 + mCherry], 128, 4 [cluster 3, R1/R2 + hChR2], 126, 4 [cluster 3, R3/R4 + mCherry], 218, 4 [clusters 0 and 3, R1/R2 + mCherry], 243, 4 [clusters 0 and 3, R1/R2 + hChR2], and 239, 4 [clusters 0 and 3, R3/R4 + mCherry]; one-way ANOVA with Tukey's test; $^{***}p < 0.001$).

SUPPLEMENTAL INFORMATION

Supplemental information can be found online at https://doi.org/10.1016/j.neuron.2023.11.012.

ACKNOWLEDGMENTS

We appreciate Dr. Maayan Schwarzkopf at Molecular Instruments for technical supports of HCR RNA-FISH experiments. This research was supported by the Brain Research Program (NRF-2017M3C7A1048089; J.W.K.) and Young Researcher Program (NRF-2020R1C1C1012788; T.-Y.C.) through the National Research Foundation of Korea, the KBRI basic research program through Korea Brain Research Institute (23-BR-04-03 and 23-BR-05-03; J.W.K.), the Ministry of Science and ICT, and the Basic Science Research Program through the NRF funded by the Ministry of Education (NRF-2017R1A6A3A01076049; T.-Y.C.).

AUTHOR CONTRIBUTIONS

Conceptualization and methodology, T.-Y.C., H.J., M.C., and J.W.K.; formal analysis, T.-Y.C., H.J., S.J., and B.K.; investigation, T.-Y.C., H.J., S.J., E.J.K., J.K., and Y.H.J.; writing – original draft, T.-Y.C.; writing – review & editing, T.-Y.C., H.J., S.J., J.K., M.C., and J.W.K.; visualization, T.-Y.C.; supervision, M.C. and J.W.K.; funding acquisition, T.-Y.C. and J.W.K.

DECLARATION OF INTERESTS

The authors declare no competing interests.

Received: February 5, 2023
Revised: September 20, 2023
Accepted: November 13, 2023
Published: December 11, 2023

REFERENCES

1. Fulenwider, H.D., Caruso, M.A., and Ryabinin, A.E. (2022). Manifestations of domination: Assessments of social dominance in rodents. Genes Brain Behav. *21*, e12731.
2. Karamihalev, S., Brivio, E., Flachskamm, C., Stoffel, R., Schmidt, M.V., and Chen, A. (2020). Social dominance mediates behavioral adaptation to chronic stress in a sex-specific manner. eLife *9*, e58723.
3. Larrieu, T., Cherix, A., Duque, A., Rodrigues, J., Lei, H., Gruetter, R., and Sandi, C. (2017). Hierarchical status predicts behavioral vulnerability and nucleus accumbens metabolic profile following chronic social defeat stress. Curr. Biol. *27*, 2202–2210.e4.
4. LeClair, K.B., Chan, K.L., Kaster, M.P., Parise, L.F., Burnett, C.J., and Russo, S.J. (2021). Individual history of winning and hierarchy landscape influence stress susceptibility in mice. eLife *10*, e71401.
5. Milewski, T.M., Lee, W., Champagne, F.A., and Curley, J.P. (2022). Behavioural and physiological plasticity in social hierarchies. Philos. Trans. R. Soc. Lond. B Biol. Sci. *377*, 20200443.
6. Murlanova, K., Kirby, M., Libergod, L., Pletnikov, M., and Pinhasov, A. (2022). Multidimensional nature of dominant behavior: Insights from behavioral neuroscience. Neurosci. Biobehav. Rev. *132*, 603–620.
7. Park, J., Ha, S., Shin, H.S., and Jeong, J. (2022). Experience of a hierarchical relationship between a pair of mice specifically influences their affective empathy toward each other. Genes Brain Behav. *21*, e12810.
8. Varholick, J.A., Pontiggia, A., Murphy, E., Daniele, V., Palme, R., Voelkl, B., Würbel, H., and Bailoo, J.D. (2019). Social dominance hierarchy type and rank contribute to phenotypic variation within cages of laboratory mice. Sci. Rep. *9*, 13650.
9. Drews, C. (1993). The concept and definition of dominance in animal behaviour. Behaviour *125*, 283–313.
10. Leimar, O., and Bshary, R. (2022). Reproductive skew, fighting costs and winner-loser effects in social dominance evolution. J. Anim. Ecol. *91*, 1036–1046.
11. Sapolsky, R.M. (2005). The influence of social hierarchy on primate health. Science *308*, 648–652.
12. Snyder-Mackler, N., Burger, J.R., Gaydosh, L., Belsky, D.W., Noppert, G.A., Campos, F.A., Bartolomucci, A., Yang, Y.C., Aiello, A.E., O'Rand, A., et al. (2020). Social determinants of health and survival in humans and other animals. Science *368*, eaax9553.
13. Ferreira-Fernandes, E., and Peça, J. (2022). The neural circuit architecture of social hierarchy in rodents and primates. Front. Cell. Neurosci. *16*, 874310.
14. Karafin, M.S., Tranel, D., and Adolphs, R. (2004). Dominance attributions following damage to the ventromedial prefrontal cortex. J. Cogn. Neurosci. *16*, 1796–1804.
15. Marsh, A.A., Blair, K.S., Jones, M.M., Soliman, N., and Blair, R.J.R. (2009). Dominance and submission: the ventrolateral prefrontal cortex and responses to status cues. J. Cogn. Neurosci. *21*, 713–724.
16. Watanabe, N., and Yamamoto, M. (2015). Neural mechanisms of social dominance. Front. Neurosci. *9*, 154.
17. Zink, C.F., Tong, Y., Chen, Q., Bassett, D.S., Stein, J.L., and Meyer-Lindenberg, A. (2008). Know your place: neural processing of social hierarchy in humans. Neuron *58*, 273–283.
18. Zhou, T., Zhu, H., Fan, Z., Wang, F., Chen, Y., Liang, H., Yang, Z., Zhang, L., Lin, L., Zhan, Y., et al. (2017). History of winning remodels thalamo-PFC circuit to reinforce social dominance. Science *357*, 162–168.
19. Padilla-Coreano, N., Batra, K., Patarino, M., Chen, Z., Rock, R.R., Zhang, R., Hausmann, S.B., Weddington, J.C., Patel, R., Zhang, Y.E., et al. (2022).

Cortical ensembles orchestrate social competition through hypothalamic outputs. Nature *603*, 667–671.

20. Wang, F., Zhu, J., Zhu, H., Zhang, Q., Lin, Z., and Hu, H. (2011). Bidirectional control of social hierarchy by synaptic efficacy in medial prefrontal cortex. Science *334*, 693–697.
21. Zhang, C., Zhu, H., Ni, Z., Xin, Q., Zhou, T., Wu, R., Gao, G., Gao, Z., Ma, H., Li, H., et al. (2022). Dynamics of a disinhibitory prefrontal microcircuit in controlling social competition. Neuron *110*, 516–531.e6.
22. Garcia-Font, N., Mitchell-Heggs, R., Saxena, K., Gabbert, C., Taylor, G., Mastroberadino, G., Spooner, P.A., Gobbo, F., Dabrowska, J.K., Chattarji, S., et al. (2022). Ca^{2+} imaging of self and other in medial prefrontal cortex during social dominance interactions in a tube test. Proc. Natl. Acad. Sci. USA *119*, e2107942119.
23. Kingsbury, L., Huang, S., Wang, J., Gu, K., Golshani, P., Wu, Y.E., and Hong, W. (2019). Correlated neural activity and encoding of behavior across brains of socially interacting animals. Cell *178*, 429–446.e16.
24. Biro, L., Sipos, E., Bruzsik, B., Farkas, I., Zelena, D., Balazsfi, D., Toth, M., and Haller, J. (2018). Task division within the prefrontal cortex: Distinct neuron populations selectively control different aspects of aggressive behavior via the hypothalamus. J. Neurosci. *38*, 4065–4075.
25. Babiczky, Á., and Matyas, F. (2022). Molecular characteristics and laminar distribution of prefrontal neurons projecting to the mesolimbic system. eLife *11*, e78813.
26. Kim, C.K., Ye, L., Jennings, J.H., Pichamoorthy, N., Tang, D.D., Yoo, A.W., Ramakrishnan, C., and Deisseroth, K. (2017). Molecular and circuit-dynamical identification of top-down neural mechanisms for restraint of reward seeking. Cell *170*, 1013–1027.e14.
27. Lui, J.H., Nguyen, N.D., Grutzner, S.M., Darmanis, S., Peixoto, D., Wagner, M.J., Allen, W.E., Kebschull, J.M., Richman, E.B., Ren, J., et al. (2021). Differential encoding in prefrontal cortex projection neuron classes across cognitive tasks. Cell *184*, 489–506.e26.
28. Murugan, M., Jang, H.J., Park, M., Miller, E.M., Cox, J., Taliaferro, J.P., Parker, N.F., Bhave, V., Hur, H., Liang, Y., et al. (2017). Combined social and spatial coding in a descending projection from the prefrontal cortex. Cell *171*, 1663–1677.e16.
29. Ma, M., Xiong, W., Hu, F., Deng, M.F., Huang, X., Chen, J.G., Man, H.Y., Lu, Y., Liu, D., and Zhu, L.Q. (2020). A novel pathway regulates social hierarchy via lncRNA AtLAS and postsynaptic synapsin IIb. Cell Res. *30*, 105–118.
30. Pallé, A., Zorzo, C., Luskey, V.E., McGreevy, K.R., Fernández, S., and Trejo, J.L. (2019). Social dominance differentially alters gene expression in the medial prefrontal cortex without affecting adult hippocampal neurogenesis or stress and anxiety-like behavior. FASEB J. *33*, 6995–7008.
31. Ghosal, S., Sandi, C., and van der Kooij, M.A. (2019). Neuropharmacology of the mesolimbic system and associated circuits on social hierarchies. Neuropharmacology *159*, 107498.
32. Hollis, F., van der Kooij, M.A., Zanoletti, O., Lozano, L., Cantó, C., and Sandi, C. (2015). Mitochondrial function in the brain links anxiety with social subordination. Proc. Natl. Acad. Sci. USA *112*, 15486–15491.
33. Shan, Q., Hu, Y., Chen, S., and Tian, Y. (2022). Nucleus accumbens dichotomically controls social dominance in male mice. Neuropsychopharmacology *47*, 776–787.
34. van der Kooij, M.A., Zalachoras, I., and Sandi, C. (2018). GABAA receptors in the ventral tegmental area control the outcome of a social competition in rats. Neuropharmacology *138*, 275–281.
35. Guenthner, C.J., Miyamichi, K., Yang, H.H., Heller, H.C., and Luo, L. (2013). Permanent genetic access to transiently active neurons via TRAP: targeted recombination in active populations. Neuron *78*, 773–784.
36. Kim, W.B., and Cho, J.H. (2017). Encoding of discriminative fear memory by input-specific LTP in the amygdala. Neuron *95*, 1129–1146.e5.
37. Samineni, V.K., Grajales-Reyes, J.G., Grajales-Reyes, G.E., Tycksen, E., Copits, B.A., Pedersen, C., Ankudey, E.S., Sackey, J.N., Sewell, S.B., Bruchas, M.R., et al. (2021). Cellular, circuit and transcriptional framework for modulation of itch in the central amygdala. eLife *10*, e68130.
38. Ye, L., Allen, W.E., Thompson, K.R., Tian, Q., Hsueh, B., Ramakrishnan, C., Wang, A.C., Jennings, J.H., Adhikari, A., Halpern, C.H., et al. (2016). Wiring and molecular features of prefrontal ensembles representing distinct experiences. Cell *165*, 1776–1788.
39. Oh, S.W., Harris, J.A., Ng, L., Winslow, B., Cain, N., Mihalas, S., Wang, Q., Lau, C., Kuan, L., Henry, A.M., et al. (2014). A mesoscale connectome of the mouse brain. Nature *508*, 207–214.
40. Krauth, N., Khalil, V., Jariwala, M., Mermet-Joret, N., Vestergaard, A.K., Capogna, M., and Nabavi, S. (2020). TRACE: an unbiased method to permanently tag transiently activated inputs. Front. Cell. Neurosci. *14*, 114.
41. Tervo, D.G., Hwang, B.Y., Viswanathan, S., Gaj, T., Lavzin, M., Ritola, K.D., Lindo, S., Michael, S., Kuleshova, E., Ojala, D., et al. (2016). A designer AAV variant permits efficient retrograde access to projection neurons. Neuron *92*, 372–382.
42. Yang, C.F., Chiang, M.C., Gray, D.C., Prabhakaran, M., Alvarado, M., Juntti, S.A., Unger, E.K., Wells, J.A., and Shah, N.M. (2013). Sexually dimorphic neurons in the ventromedial hypothalamus govern mating in both sexes and aggression in males. Cell *153*, 896–909.
43. Broussard, G.J., Liang, Y., Fridman, M., Unger, E.K., Meng, G., Xiao, X., Ji, N., Petreanu, L., and Tian, L. (2018). In vivo measurement of afferent activity with axon-specific calcium imaging. Nat. Neurosci. *21*, 1272–1280.
44. Chou, Y.J., Lu, Y.H., Ma, Y.K., Su, Y.S., and Kuo, T.H. (2021). The decisive role of subordination in social hierarchy in weanling mice and young children. iScience *24*, 102073.
45. Ilia, M. (2004). Oct-6 transcription factor. Int. Rev. Neurobiol. *59*, 471–489.
46. Meijer, D., Graus, A., Kraay, R., Langeveld, A., Mulder, M.P., and Grosveld, G. (1990). The octamer binding factor Oct6: cDNA cloning and expression in early embryonic cells. Nucleic Acids Res. *18*, 7357–7365.
47. Monuki, E.S., Weinmaster, G., Kuhn, R., and Lemke, G. (1989). SCIP: a glial POU domain gene regulated by cyclic AMP. Neuron *3*, 783–793.
48. Suzuki, N., Rohdewohld, H., Neuman, T., Gruss, P., and Schöler, H.R. (1990). Oct-6: a POU transcription factor expressed in embryonal stem cells and in the developing brain. EMBO J. *9*, 3723–3732.
49. Zhu, Q., Song, L., Peng, G., Sun, N., Chen, J., Zhang, T., Sheng, N., Tang, W., Qian, C., Qiao, Y., et al. (2014). The transcription factor Pou3f1 promotes neural fate commitment via activation of neural lineage genes and inhibition of external signaling pathways. eLife *3*, e02224.
50. Lee, B.K., Jang, Y.J., Kim, M., LeBlanc, L., Rhee, C., Lee, J., Beck, S., Shen, W., and Kim, J. (2019). Super-enhancer-guided mapping of regulatory networks controlling mouse trophoblast stem cells. Nat. Commun. *10*, 4749.
51. Matsuda, K., Mikami, T., Oki, S., Iida, H., Andrabi, M., Boss, J.M., Yamaguchi, K., Shigenobu, S., and Kondoh, H. (2017). ChIP-seq analysis of genomic binding regions of five major transcription factors highlights a central role for ZIC2 in the mouse epiblast stem cell gene regulatory network. Development *144*, 1948–1958.
52. Kauer, J.A., and Malenka, R.C. (2007). Synaptic plasticity and addiction. Nat. Rev. Neurosci. *8*, 844–858.
53. Russo, S.J., and Nestler, E.J. (2013). The brain reward circuitry in mood disorders. Nat. Rev. Neurosci. *14*, 609–625.
54. van der Kooij, M.A., Hollis, F., Lozano, L., Zalachoras, I., Abad, S., Zanoletti, O., Grosse, J., Guillot de Suduiraut, I., Canto, C., and Sandi, C. (2018). Diazepam actions in the VTA enhance social dominance and mitochondrial function in the nucleus accumbens by activation of dopamine D1 receptors. Mol. Psychiatry *23*, 569–578.
55. Ghosal, S., Gebara, E., Ramos-Fernández, E., Chioino, A., Grosse, J., Guillot de Suduiraut, I., Zanoletti, O., Schneider, B., Zorzano, A., Astori, S., et al. (2023). Mitofusin-2 in nucleus accumbens D2-MSNs regulates social dominance and neuronal function. Cell Rep. *42*, 112776.

56. Bonini, F., Burle, B., Liégeois-Chauvel, C., Régis, J., Chauvel, P., and Vidal, F. (2014). Action monitoring and medial frontal cortex: leading role of supplementary motor area. Science *343*, 888–891.

57. Saunders, B., Lin, H., Milyavskaya, M., and Inzlicht, M. (2017). The emotive nature of conflict monitoring in the medial prefrontal cortex. Int. J. Psychophysiol. *119*, 31–40.

58. Vertes, R.P. (2006). Interactions among the medial prefrontal cortex, hippocampus and midline thalamus in emotional and cognitive processing in the rat. Neuroscience *142*, 1–20.

59. He, X., Treacy, M.N., Simmons, D.M., Ingraham, H.A., Swanson, L.W., and Rosenfeld, M.G. (1989). Expression of a large family of POU-domain regulatory genes in mammalian brain development. Nature *340*, 35–41.

60. Fyodorov, D., and Deneris, E. (1996). The POU domain of SCIP/Tst-1/Oct-6 is sufficient for activation of an acetylcholine receptor promoter. Mol. Cell. Biol. *16*, 5004–5014.

61. Ilia, M., Bazigou, E., and Price, J. (2003). Expression of the POU domain transcription factor, Oct-6, is attenuated in the adult mouse telencephalon, but increased by neurotoxic damage. Exp. Neurol. *181*, 159–169.

62. Bhattacherjee, A., Djekidel, M.N., Chen, R., Chen, W., Tuesta, L.M., and Zhang, Y. (2019). Cell type-specific transcriptional programs in mouse prefrontal cortex during adolescence and addiction. Nat. Commun. *10*, 4169.

63. Chen, R., Liu, Y., Djekidel, M.N., Chen, W., Bhattacherjee, A., Chen, Z., Scolnick, E., and Zhang, Y. (2022). Cell type-specific mechanism of Setd1a heterozygosity in schizophrenia pathogenesis. Sci. Adv. *8*, eabm1077.

64. Co, M., Hickey, S.L., Kulkarni, A., Harper, M., and Konopka, G. (2020). Cortical Foxp2 supports behavioral flexibility and developmental dopamine D1 receptor expression. Cereb. Cortex *30*, 1855–1870.

65. Ma, S., Skarica, M., Li, Q., Xu, C., Risgaard, R.D., Tebbenkamp, A.T.N., Mato-Blanco, X., Kovner, R., Krsnik, Ž., de Martin, X., et al. (2022). Molecular and cellular evolution of the primate dorsolateral prefrontal cortex. Science *377*, eabo7257.

66. Renner, K., Sock, E., Bermingham, J.R., and Wegner, M. (1996). Expression of the gene for the POU domain transcription factor Tst-1/Oct6 is regulated by an estrogen-dependent enhancer. Nucleic Acids Res. *24*, 4552–4557.

67. Nakata, M., Ågmo, A., Sagoshi, S., and Ogawa, S. (2018). The role of estrogen receptor β (ERβ) in the establishment of hierarchical social relationships in male mice. Front. Behav. Neurosci. *12*, 245.

68. Pelkey, K.A., Barksdale, E., Craig, M.T., Yuan, X., Sukumaran, M., Vargish, G.A., Mitchell, R.M., Wyeth, M.S., Petralia, R.S., Chittajallu, R., et al. (2015). Pentraxins coordinate excitatory synapse maturation and circuit integration of parvalbumin interneurons. Neuron *85*, 1257–1272.

69. Xiao, M.F., Roh, S.E., Zhou, J., Chien, C.C., Lucey, B.P., Craig, M.T., Hayes, L.N., Coughlin, J.M., Leweke, F.M., Jia, M., et al. (2021). A biomarker-authenticated model of schizophrenia implicating NPTX2 loss of function. Sci. Adv. *7*, eabf6935.

70. Naeve, G.S., Ramakrishnan, M., Kramer, R., Hevroni, D., Citri, Y., and Theill, L.E. (1997). Neuritin: a gene induced by neural activity and neurotrophins that promotes neuritogenesis. Proc. Natl. Acad. Sci. USA *94*, 2648–2653.

71. Son, H., Banasr, M., Choi, M., Chae, S.Y., Licznerski, P., Lee, B., Voleti, B., Li, N., Lepack, A., Fournier, N.M., et al. (2012). Neuritin produces antidepressant actions and blocks the neuronal and behavioral deficits caused by chronic stress. Proc. Natl. Acad. Sci. USA *109*, 11378–11383.

72. Schwenk, J., Harmel, N., Zolles, G., Bildl, W., Kulik, A., Heimrich, B., Chisaka, O., Jonas, P., Schulte, U., Fakler, B., et al. (2009). Functional proteomics identify cornichon proteins as auxiliary subunits of AMPA receptors. Science *323*, 1313–1319.

73. Herring, B.E., Shi, Y., Suh, Y.H., Zheng, C.Y., Blankenship, S.M., Roche, K.W., and Nicoll, R.A. (2013). Cornichon proteins determine the subunit composition of synaptic AMPA receptors. Neuron *77*, 1083–1096.

74. Bruno, C.A., O'Brien, C., Bryant, S., Mejaes, J.I., Estrin, D.J., Pizzano, C., and Barker, D.J. (2021). pMAT: An open-source software suite for the analysis of fiber photometry data. Pharmacol. Biochem. Behav. *201*, 173093.

75. Zheng, G.X., Terry, J.M., Belgrader, P., Ryvkin, P., Bent, Z.W., Wilson, R., Ziraldo, S.B., Wheeler, T.D., McDermott, G.P., Zhu, J., et al. (2017). Massively parallel digital transcriptional profiling of single cells. Nat. Commun. *8*, 14049.

76. Stuart, T., Butler, A., Hoffman, P., Hafemeister, C., Papalexi, E., Mauck, W.M., 3rd, Hao, Y., Stoeckius, M., Smibert, P., and Satija, R. (2019). Comprehensive integration of single-cell data. Cell *177*, 1888–1902.e21.

77. Fan, Z., Zhu, H., Zhou, T., Wang, S., Wu, Y., and Hu, H. (2019). Using the tube test to measure social hierarchy in mice. Nat. Protoc. *14*, 819–831.

78. Hitti, F.L., and Siegelbaum, S.A. (2014). The hippocampal CA2 region is essential for social memory. Nature *508*, 88–92.

79. Ahn, S., Kang, Y., Lee, J.W., Jeong, S.J., Lee, Y.J., Lee, S., Kim, J., Koo, J.W., Kim, J.J., and Jung, M.W. (2021). A role of anterior cingulate cortex in the emergence of worker-parasite relationship. Proc. Natl. Acad. Sci. USA *118*, e2111145118.

80. Choi, T.Y., Lee, S.H., Kim, Y.J., Bae, J.R., Lee, K.M., Jo, Y., Kim, S.J., Lee, A.R., Choi, S., Choi, L.M., et al. (2018). Cereblon maintains synaptic and cognitive function by regulating BK channel. J. Neurosci. *38*, 3571–3583.

81. Kim, J., Kang, S., Choi, T.Y., Chang, K.A., and Koo, J.W. (2022). Metabotropic glutamate receptor 5 in amygdala target neurons regulates susceptibility to chronic social stress. Biol. Psychiatry *92*, 104–115.

82. Noh, K., Lee, H., Choi, T.Y., Joo, Y., Kim, S.J., Kim, H., Kim, J.Y., Jahng, J.W., Lee, S., Choi, S.Y., et al. (2019). Negr1 controls adult hippocampal neurogenesis and affective behaviors. Mol. Psychiatry *24*, 1189–1205.

83. Cadwell, C.R., Scala, F., Li, S., Livrizzi, G., Shen, S., Sandberg, R., Jiang, X., and Tolias, A.S. (2017). Multimodal profiling of single-cell morphology, electrophysiology, and gene expression using Patch-seq. Nat. Protoc. *12*, 2531–2553.

84. Jennings, J.H., Rizzi, G., Stamatakis, A.M., Ung, R.L., and Stuber, G.D. (2013). The inhibitory circuit architecture of the lateral hypothalamus orchestrates feeding. Science *341*, 1517–1521.

85. Lee, J.H., Ribeiro, E.A., Kim, J., Ko, B., Kronman, H., Jeong, Y.H., Kim, J.K., Janak, P.H., Nestler, E.J., Koo, J.W., et al. (2020). Dopaminergic regulation of nucleus accumbens cholinergic interneurons demarcates susceptibility to cocaine addiction. Biol. Psychiatry *88*, 746–757.

86. Lipovsek, M., Browne, L., and Grubb, M.S. (2020). Protocol for Patch-seq of small interneurons. Star Protoc. *1*, 100146.

87. Livak, K.J., and Schmittgen, T.D. (2001). Analysis of relative gene expression data using real-time quantitative PCR and the 2(-Delta Delta C(T)) method. Methods *25*, 402–408.

88. Vandrey, B., Armstrong, J., Brown, C.M., Garden, D.L.F., and Nolan, M.F. (2022). Fan cells in lateral entorhinal cortex directly influence medial entorhinal cortex through synaptic connections in layer 1. eLife *11*, e83008.

89. Beier, K.T., Kim, C.K., Hoerbelt, P., Hung, L.W., Heifets, B.D., DeLoach, K.E., Mosca, T.J., Neuner, S., Deisseroth, K., Luo, L., et al. (2017). Rabies screen reveals GPe control of cocaine-triggered plasticity. Nature *549*, 345–350.

90. Aran, D., Looney, A.P., Liu, L., Wu, E., Fong, V., Hsu, A., Chak, S., Naikawadi, R.P., Wolters, P.J., Abate, A.R., et al. (2019). Reference-based analysis of lung single-cell sequencing reveals a transitional profibrotic macrophage. Nat. Immunol. *20*, 163–172.

91. Yan, Y., Tian, M., Li, M., Zhou, G., Chen, Q., Xu, M., Hu, Y., Luo, W., Guo, X., Zhang, C., et al. (2022). ASH1L haploinsufficiency results in autistic-like phenotypes in mice and links Eph receptor gene to autism spectrum disorder. Neuron *110*, 1156–1172.e9.

Please cite this article in press as: Choi et al., Distinct prefrontal projection activity and transcriptional state conversely orchestrate social competition and hierarchy, Neuron (2023), https://doi.org/10.1016/j.neuron.2023.11.012

STAR★METHODS

KEY RESOURCES TABLE

REAGENT or RESOURCE	SOURCE	IDENTIFIER
Antibodies		
Rabbit monoclonal anti-c-Fos	Cell Signaling Technology	Cell Signaling Technology Cat# 2250; RRID:AB_2247211
Rabbit polyclonal anti-Pou3f1	Abcam	Abcam Cat# ab272925; RRID:AB_2927579
Donkey anti-rabbit, Alexa Fluor 647 Conjugated	Molecular Probes	Molecular Probes Cat# A-31573; RRID:AB_2536183
Donkey anti-rabbit, Alexa Fluor 555 Conjugated	Thermo Fisher Scientific	Thermo Fisher Scientific Cat# A-31572; RRID:AB_162543
Bacterial and virus strains		
AAV1-phSyn1-FLEX-tdTomato-T2A-SypEGFP-WPRE	Addgene	51509-AAV1
AAVrg-EF1a-DIO-EYFP-WPRE-pA	UNC Vector Core	N/A
AAVrg-EF1a-DIO-mCherry	UNC Vector Core	N/A
AAVrg-hSyn-EGFP	Addgene	50465-AAVrg
AAVrg-hSyn-mCherry	Addgene	114472-AAVrg
AAV2-EF1a-DIO-EYFP-WPRE-pA	UNC Vector Core	N/A
AAV2-Flex-taCasp3-TEVp	UNC Vector Core	N/A
rAAV2-Retro-EF1a-mCherry-IRES-Cre	Addgene	55632-AAVrg
AAV5-CaMKIIa-EYFP	UNC Vector Core	N/A
AAV5-CaMKIIa-hChR2(H134R)-EYFP	UNC Vector Core	N/A
AAV5-cFos-ERT2-Cre-ERT2-Pest-p2a-no WPRE	UNC Vector Core	N/A
AAVrg-CAG-tdTomato	UNC Vector Core	N/A
AAV5-EF1a-DIO-eNpHR3.0-EYFP	UNC Vector Core	N/A
AAV9-hSyn1-axon-GCaMP6s-P2A-mRuby3	Addgene	112005-AAV9
AAVrg-hSyn-TagBFP2	VectorBuilder	N/A
AAV2-CMV-Flex-scrambled shRNA-EGFP	VectorBuilder	N/A
AAV2-CMV-Flex-*Pou3f1* shRNA-EGFP	VectorBuilder	N/A
AAV2-CAG-Flex-EGFP-WPRE	Addgene	51502-AAV2
AAV2-CMV-Flex-*Pou3f1*-P2A-EGFP-WPRE	VectorBuilder	N/A
AAVrg-CAG-Cre	UNC Vector Core	N/A
AAV5-EF1a-DIO-EYFP-WPRE-pA	UNC Vector Core	N/A
AAV5-EF1a-DIO-hChR2(H134R)-EYFP	UNC Vector Core	N/A
AAV5-EF1a-DIO-mCherry	UNC Vector Core	N/A
AAV5-EF1a-DIO-hChR2(H134R)-mCherry	UNC Vector Core	N/A
Chemicals, peptides, and recombinant proteins		
Isoflurane	Hana Pharm	N/A
Tissue-Plus™ O.C.T. Compound	Fisher Scientific	FIS23-730-571
4-hydroxytamoxifen	Sigma-Aldrich	H6278
Hibernate A without calcium & Magnesium	Brainbits	HA-CaMg500
Papain	Worthington	LS003120
D-(+)-Trehalose dihydrate	Sigma-Aldrich	T0167
DL-2-amino-5-phosphonopentanoic acid	Sigma-Aldrich	A5282
DNase I	NEB	M0303L
Critical commercial assays		
Sing Cell-to-CT™ qRT-PCR kit	Invitrogen	4458237

(*Continued on next page*)

Please cite this article in press as: Choi et al., Distinct prefrontal projection activity and transcriptional state conversely orchestrate social competition and hierarchy, Neuron (2023), https://doi.org/10.1016/j.neuron.2023.11.012

Continued

REAGENT or RESOURCE	SOURCE	IDENTIFIER
Chromium Single Cell 3' GEM, Library & Gel Bead Kit v3	10x Genomics	1000075
Chromium i7 Multiplex Kit	10x Genomics	120262
Chromium Chip B Single Cell Kit	10x Genomics	1000073
HCR™ RNA-FISH Buffers, Amplifiers and Probe sets	Molecular Instruments	N/A
Deposited data		
scRNA-seq data	This paper	GEO: GSE222185
Experimental models: Organisms/strains		
Mouse: C57BL/6N	Orient Bio, Busan, Rep. of Korea	N/A
Mouse: *Fos*^{creER} (B6.129(Cg)-Fostm1.1(cre/ERT2)Luo/J)	The Jackson Laboratory	RRID:IMSR_JAX:021882
Mouse: *Ai6* B6.Cg-Gt(ROSA)26Sortm6(CAG-ZsGreen1)Hze/J	The Jackson Laboratory	RRID:IMSR_JAX:007906
Oligonucleotides		
Taqman gene expression assay: *Nptx2*	Thermo Fisher Scientific	Mm00479438_m1
Taqman gene expression assay: *Nrn1*	Thermo Fisher Scientific	Mm00467844_m1
Taqman gene expression assay: *Cnih3*	Thermo Fisher Scientific	Mm01319298_m1
Taqman gene expression assay: *Ankrd33b*	Thermo Fisher Scientific	Mm07298789_m1
Taqman gene expression assay: *Mpv17*	Thermo Fisher Scientific	Mm00485133_m1
Taqman gene expression assay: *Nrip3*	Thermo Fisher Scientific	Mm00508049_m1
Taqman gene expression assay: *Pou3f1*	Thermo Fisher Scientific	Mm00843534_s1
Taqman gene expression assay: *Ly6a*	Thermo Fisher Scientific	Mm00726565_s1
Taqman gene expression assay: *Rn18s*	Thermo Fisher Scientific	Mm03928990_g1
Software and algorithms		
ImageJ (Fiji)	NIH	v1.53
SlideViewer	3D HISTECH	v2.7
Leica Application Suite X (LAS X)	Leica	2.0.0.14332
Doric Neuroscience Studio	Doric Lens	v5.3.3.14
pMAT	Bruno et al.[74]	v1.2
pClamp	Molecular Devices	v10
SMART	Panlab Harvard Apparatus	v3.0
WEKA	The University of Waikato	v3.8.6
10x Genomics Cell Ranger 4.0.0	Zheng et al.[75]	N/A
Seurat package 3.1.3 in R	Stuart et al.[76]	N/A
Graphpad Prism	GraphPad	v10
Other		
Fiber optic cannula for optogenetics (200 mm diameter, 0.22 NA)	RWD	R-FOC-L200C-22NA
Fiber optic cannula for fiber photometry (400 mm diameter, 0.50 NA)	RWD	R-FOC-BL400C-50NA
Dental Cement	Dentsply Sirona	Poly-F
VECTASIELD HardSet Antifade Mounting Medium with DAPI	Vector Laboratories	H-1500
VectaMount Permanent Mounting Medium	Vector Laboratories	H-5000
DAPI Solution (1 mg/mL)	Thermo Scientific	62248
Cholera Toxin Subunit B, Alexa Fluor™ 647 Conjugated (CTB-647)	Invitrogen™	C34778

Please cite this article in press as: Choi et al., Distinct prefrontal projection activity and transcriptional state conversely orchestrate social competition and hierarchy, Neuron (2023), https://doi.org/10.1016/j.neuron.2023.11.012

RESOURCE AVAILABILITY

Lead contact

Further information and requests for resources and reagents should be directed to and will be fulfilled by the Lead Contact, Ja Wook Koo (jawook.koo@kbri.re.kr).

Materials availability

This study did not generate new unique reagents.

Data and code availability

- scRNA-seq data is deposited at NCBI's Gene Expression Omnibus, and is publicly available through GEO Series accession number GSE222185.
- This paper does not report original code.
- Any additional information required to reanalyze the data reported in this paper is available from the lead contact upon request.

EXPERIMENTAL MODEL AND STUDY PARTICIPANT DETAILS

Animals

Adult (over 2 months old) male C57BL/6N, *Fos*^{CreER} and *Ai6* mice were used for experiments. Mice of similar body weight within 10 percent differences and ages within a week of birth date were housed in cages of 2-4 for at least two weeks before surgical manipulations or behavioral experiments, maintained in an animal facility with a specific pathogen-free barrier under a 12-h light/dark cycle (lights on at 08:00 am), the temperature at 22 ± 2 °C and the humidity at 50 ± 10%, and given access to food and water *ad libitum*. All surgical manipulations and behavioral tests were carried out in the animal facility during their light on period, specifically ZT 04:00 ~ ZT 12:00. The Institutional Animal Care and Use Committee (IACUC) at Korea Brain Research Institute authorized all procedures (IACUC-21-00039). The use of male only mice limits the generalizability of the results. Only health and immunocompetent mice were used. The health status of mice, including body weight, fur loss, and wounds, were monitored from the beginning to the end of the experiment. Animals with any health abnormalities were excluded from the experiment. Mice in this study were drug and test naïve and not involved in any previous procedures.

METHOD DETAILS

Stereotaxic surgeries

Mice were deeply anesthetized by an intraperitoneal injection of 0.1M phosphate-buffered saline (PBS) containing ketamine (100 mg/kg) and xylazine (10 mg/kg). The head of a deeply anesthetized mouse was fixed in a stereotaxic apparatus (Stoelting Co.), and the eyes were coated with ophthalmic ointment to avoid eye dryness. Scalp hair was removed, and the skin was cleaned with Betadine. Fine surgical scissors were used to make a midline incision to expose the skull, and a microdrill was used to make the craniotomies above the locations where viral vectors were injected or fiber optic cannulas were implanted. For all injections, a 5-μL microsyringe (7641-01, Hamilton) connected with a 33-gauge needle (7762-06, Hamilton) was used. Viral vectors were injected at a rate of 100 nL/min, and the needle was kept in place for an additional 10 min to allow for viral dispersion before being removed. The scalp incision was closed with a surgical suture and tissue adhesive (Vetbont, 3M). For implanting fiber optic cannula, dental cement was applied to secure them. All stereotaxic coordinates were measured relative to bregma. After surgery, mice recovered in a clean cage under a heat lamp until awakening from anesthesia. Before undergoing subsequent operations or behavioral tests, mice were given a minimum of two weeks to recuperate.

For tracing activated mPFC neurons and their projections (Figures 1A–1E and S1A–S1C), *Fos*^{CreER} mice were bilaterally injected with 500 nL of AAV1-phSyn1-FLEX-tdTomato-T2A-SypEGFP into the mPFC (anteroposterior (AP), +2.1 mm; mediolateral (ML), ±0.6 mm; dorsoventral (DV), -2.1 mm; angle, 10°).

For TRACE experiments (Figures 1F–1H), *Fos*^{CreER} mice were bilaterally injected 500 nL of AAVrg-EF1a-DIO-EYFP into the NAc (AP, +1.3 mm; ML, ±1.6 mm; DV, -4.6 mm; angle, 10°) and 500 nL of AAVrg-EF1a-DIO-mCherry into the VTA (AP, -3.2 mm; ML, ±1.2 mm; DV, -4.6 mm; angle, 10°).

For retrograde tracing experiments (Figures 5C–5F, S1D–S1J, S2, S6G–S6K, and S7), C57BL/6N mice were bilaterally injected 500 nL of AAVrg-hSyn-EGFP, AAVrg-CAG-tdTomato, AAVrg-hSyn-mCherry, AAVrg-hSyn-TagBFP2 or CTB-647 into the NAc (AP, +1.3 mm; ML, ±1.6 mm; DV, -4.6 mm; angle, 10°) and/or the VTA (AP, -3.2 mm; ML, ±1.2 mm; DV, -4.6 mm; angle, 10°).

For fiber photometry experiments (Figures 2 and S3), 500 nL of AAV9-hSyn1-axon-GCaMP6s-P2A-mRuby3 was injected into the right mPFC (AP, +2.1 mm; ML, +0.3 mm; DV, -2.0 mm; angle, 0°) of C57BL/6N mice. Fiber optic cannula (400 μm core diameter, 0.50 NA; RWD Life Science) were implanted into the right NAc (AP, +1.3 mm; ML, +0.8 mm; DV, -4.2 mm; angle, 0°) and VTA (AP, -3.2 mm; ML, +1.2 mm; DV, -4.4 mm; angle, 10°) on the same day or several days after the virus injection.

For genetic ablation experiments (Figures 3A–3H and S4A–S4F), C57BL/6N mice were bilaterally injected 500 nL of AAVrg-EF1a-mCherry-IRES-Cre into the NAc (AP, +1.3 mm; ML, ±1.6 mm; DV, -4.6 mm; angle, 10°) or the VTA (AP, -3.2 mm; ML, ±1.2 mm; DV, -4.6 mm; angle, 10°) and 500 nL of AAV2-EF1a-Flex-taCasp3-TEVp or AAV2-EF1a-DIO-EYFP into the mPFC (AP, +2.1 mm; ML, ±0.6 mm; DV, -2.1 mm; angle, 10°).

For mPFC terminal activation experiments (Figures 3I–3T and S5), C57BL/6N mice were uni- or bilaterally injected 500 nL of AAV5-CaMKIIa-hChR2(H134R)-EYFP or AAV5-CaMKIIa-EYFP into the mPFC (AP, +2.1 mm; ML, ±0.3 mm; DV, -2.0 mm; angle, 0°), and fiber optic cannula (200 μm core diameter, 0.22 numerical aperture (NA); RWD Life Science) were implanted into the NAc (AP, +1.3 mm; ML, +0.8 mm; DV, -4.2 mm; angle, 0°) or VTA (AP, -3.2 mm; ML, +0.4 mm; DV, -4.3 mm; angle, 0°) on the same day or several days after virus injection.

For labeling activated neurons with retrograde tracing (Figures S4G–S4O), *Ai6* mice were bilaterally injected 500 nL of AAV5-cFos-ER^{T2}-Cre-ER^{T2} in the mPFC (AP, +2.1 mm; ML, ±0.6 mm; DV, -2.1 mm; angle, 10°), AAVrg-CAG-tdTomato in the NAc (AP, +1.3 mm; ML, ±1.6 mm; DV, -4.6 mm; angle, 10°) and CTB-647 in the VTA (AP, -3.2 mm; ML, ±1.2 mm; DV, -4.6 mm; angle, 10°).

For inhibition of activated mPFC projections (Figures S4P–S4Z), 600 nL of a mixture of two viruses (AAV5-cFos-ER^{T2}-Cre-ER^{T2} and AAV5-EF1a-DIO-NpHR3.0-EYFP, ratio, 1:1) was injected into the mPFC (AP, +2.1 mm; ML, +0.3 mm; DV, -2.0 mm; angle, 0° (left) and AP, +2.1 mm; ML, +0.6 mm; DV, -2.1 mm; angle, 10° (right)), and fiber optic cannula were implanted into the NAc (AP, +1.3 mm; ML, +0.8 mm; DV, -4.3 mm; angle, 0° (left) and AP, +1.3 mm; ML, ±1.6 mm; DV, -4.4 mm; angle, 10° (right)) or VTA (AP, -3.2 mm; ML, +0.4 mm; DV, -4.3 mm; angle, 0° (left) and AP, -3.2 mm; ML, +1.2 mm; DV, -4.4 mm; angle, 10° (right)) on the same day or several days after virus injection.

For projection-specific genetic manipulation experiments (Figures 6 and S9), C57BL/6N mice were bilaterally injected 500 nL of AAVrg-CAG-Cre into the VTA (AP, -3.2 mm; ML, ±1.2 mm; DV, -4.6 mm; angle, 10°) and 500 nL of AAV2-CMV-Flex-*Pou3f1* shRNA-EGFP-WPRE, AAV2-CMV-Flex-scrambled shRNA-EGFP, AAV2-CMV-Flex-*Pou3f1*-P2A-EGFP-WPRE, or AAV2-CAG-Flex-EGFP-WPRE into the mPFC (AP, +2.1 mm; ML, ±0.6 mm; DV, -2.1 mm; angle, 10°). A social subordinate (R3 or R4; for Figures 6B–6G and S9A–S9D) or dominant animal (R1 or R2; for Figures 6H–6M and S9E–S9H), which received viral injections, was housed together in the same cage with other three cagemates that received control virus. These four mice were co-housed in a single home cage for four weeks to allow for full expression of the transgenes.

For mPFC-VTA cell body activation experiments (Figures 7 and S10), C57BL/6N mice were bilaterally injected 500 nL of AAVrg-CAG-Cre into the VTA (AP, -3.2 mm; ML, ±1.2 mm; DV, -4.6 mm; angle, 10°) and 500 nL of AAV5-EF1a-DIO-hChR2(H134R)-EYFP (or mChery) or AAV5-EF1a-DIO-EYFP (or mCherry) into the mPFC (AP, +2.1 mm; ML, ±0.6 mm; DV, -2.1 mm; angle, 10°). Fiber optic cannula were bilaterally implanted 200 μm above the viral injection coordinates of the mPFC on the same day or several days after the virus injection.

Animals were excluded from the data analysis if the viral vector expresses at an inaccurate location or if the fiber optic cannula is implanted at an inaccurate location.

Behavioral assays

Tube test

The tube test was conducted as instructed with minor modifications.[18,20,77] Mice were softly handled for at least 2 days (2 min/day) before the tube test to acclimate them to the experimenters and minimize stress and then trained to pass through the transparent acrylic tube with a 3-cm inner diameter and 30-cm length for 10 trials per day. On test days, two mice were released from the opposite sides of a tube, met at the center, and the mouse who withdrew first from the tube was declared as the "loser". One more test with the same pair of mice was conducted after at least 1 min. Mice were released at the opposite ends of the tube. It was considered a draw if the different mouse alternately wins in two repeated tests of the same pairs. For a set of 4 mice, the 6 pairs of mice were tested daily using a round-robin design in a random sequence, and the total number of wins on each test day was used to establish the social rank of the animals. If the same rank position in a cage did not change for the final two-thirds of the test time, this cage was used for further manipulation experiments.

For tracing activated mPFC neurons and projections (Figures 1A–1E and S1A–S1C) or TRACE experiments (Figures 1F–1H), three mice were housed together in a cage for at least two weeks after virus injection and recovery. We conducted the same handling and tube training procedures (described above) for all mice. The tube test was repeated 10 times with a 1-min interval between the randomly selected pair of mice in a cage. The control mouse, which remained in the same cage, was permitted to cross the tube 10 times without competition with another mouse. 4-hydroxytamoxifen (H6278, Sigma-Aldrich; 10 mg/kg) was intraperitoneally injected at 2 hours after the tube test.[38,40] After the behavioral tests, all mice were kept separately for a further 2 (for TRACE experiments) or 4 weeks (for tracing activated mPFC neurons and projections) to avoid the labeled neurons and projections activated by various social interactions under group housing and to fully express fluorophore.

For genetic ablation experiments (Figures 3A–3H and S4A–S4F), a mouse that was injected viral vectors for projection-specific genetic ablation and another one that was injected viral vectors to express projection-specific fluorescent proteins were housed in a cage for at least 2 weeks after virus injection and recovery, and these 2 mice were conducted the same procedure of the tube test (described above) for 3 consecutive days to determine winner and loser.

For fiber photometry or optogenetic manipulation experiments, the same diameter and length tube with a 12 mm open slit on the top was used to pass the mice connected to the patchcords. Patchcords were connected to all mice at least 30 min before the

Please cite this article in press as: Choi et al., Distinct prefrontal projection activity and transcriptional state conversely orchestrate social competition and hierarchy, Neuron (2023), https://doi.org/10.1016/j.neuron.2023.11.012

training and test. For fiber photometry experiments (Figures 2 and S3), a modified tube with a movable door at the middle of the tube was used. Mice in the tube started to compete when a door was removed after 10 s delay period to avoid any obstructions from the uncontrollable moving of mice in the tube or human handling. For optogenetic activation experiments (Figures 3I–3T, 7A–7F, S5, S10A, and S10B), the tube test ranks were verified once again before optogenetic stimulation, and blue light stimulation (473 nm, 1 ∼ 20 mW (for hChR2 experiments of Figures 3I–3T and S5A–S5G) or 10 mW (for control experiments of Figures 3I–3T, 7A–7F, S5A—S5S, S10A, and S10B) at the tip of the optical fiber; 10 ms pulses at 20 Hz for Figures 3I–3T, S5A–S5G or at 10 Hz for Figures 7A–7F, S10A, and S10B) was used. For Figures 3I–3T and S5A–S5G, the light intensity of 1 mW was delivered at the first trial of optogenetic activation experiment, and it was steadily increased in the next trial if the rank was not changed (1-3-5-7-10-15-20 mW). The light intensity was not altered during the tube test sessions. If the rank did not change, the next tube test was performed after 5-min rest. If the rank was not altered by the maximal light intensity (20 mW), tests for this animal were terminated. For optogenetic inhibition experiments (Figures S4P–S5Z), the tube test ranks were verified once again before optogenetic stimulation, and constant green light stimulation (532 nm, 10 mW at the tip of the optical fiber) was delivered from right before mice entering the tube throughout the test. For optogenetic activation during the tube test with a dummy mouse (Figures S5M–S5S), a mouse did the tube test with a dummy mouse that is positioned in opposite side in the tube. Blue light stimulation (473 nm, 10 mW at the tip of the optical fiber; 10 ms pulses at 20 Hz) was delivered from right before mice entering the tube throughout the test.

With the exception of the tube test with fiber photometry recordings, all tube tests were videotaped using a webcam (C922, Logitech), and recordings of each tube test were blindly evaluated frame by frame. Five forms of behaviors during the tube test were manually annotated: 1) approach (either or both mice moved toward each other), 2) push (a mouse actively shoved the opponent), 3) resistance (a mouse held on the territory when being pushed by the opponent), 4) active retreat (a mouse voluntarily walked backward without pushes or approaches of the opponent) and 5) passive approach (a mouse backed away by pushes of the opponent). The number of each behavior during an entire tube test session was counted.

Direct social interaction test

This test was carried out with slight modifications as described in a prior study.[78] Mice were habituated at least 30 min prior in a behavior room under standard room light. A novel mouse (C57BL/6N, 5-6-week-old, male) was introduced in a home cage that was housing an experimental mouse. The total amount of social contacts of an experimental mouse, including anogenital and nose-to-nose sniffing, following, and allogrooming, was measured for 5 min.

Open field test (OFT)

Mice were individually entered in the center zone of OFT chamber (42 × 42 cm) for 10 min. Animals' behaviors were recorded by a video camera and analyzed with the SMART 3.0 software (Panlab Harvard Apparatus). 473 nm blue laser light was intermittently turned on and off on the test mice with 1 min epochs. Total distance and time in the center per minute were analyzed.

Wet bedding avoidance test

A rectangular plastic cage (20 cm X 35 cm) with new bedding was placed in the open field test box (40 cm X 40 cm) to block visual cues around the cage, and 250-300 mL of clean water was poured into the cage to fully dampen the bedding. A cylindrical acrylic platform (5 cm diameter and 5 cm height) was placed in the center of the cage. Four mice from the same cage were first entered into a cage with wet bedding, and all mice were briefly put on the platform for a while to make the mice recognize it and then lower them back to the floor. Behaviors of the four mice in the cage with wet bedding were videotaped for 20 min using a webcam (C922, Logitech). Each animal's platform occupancy duration was then measured manually. The criterion of the occupancy is that the four legs of the mouse must be on the platform.

Histology and image acquisition

Animals were deeply anesthetized with CO_2 and transcardially perfused with 0.1 M phosphate-buffered saline (PBS) and 4% (wt/vol) paraformaldehyde (PFA) in PBS. Brains were removed, post-fixed overnight in 4% PFA, and equilibrated in 30% sucrose in PBS at 4°C. 20 (for fluorescence *in situ* hybridization (FISH) experiments) or 50-60 μm thick coronal sections (for other histological experiments) were cut on a cryocut microtome (CM1860, Leica Biosystems) at -20°C.

To quantify activated mPFC neurons and their projections (Figures 1A–1E and S1A–S1C), all brain sections were washed in PBS, mounted on slide glasses (Muto pure chemicals) and cover-slipped with VECTASIELD HardSet Antifade Mounting Medium with DAPI (H-1500, Vector Laboratories). Images were acquired using a confocal microscope (TCS SP8, Leica) with a 20X (for mPFC) or 63X (for other brain areas) objective lens.

Immunostaining of c-Fos and quantification (Figures S1D–S1J) were carried out as previously reported with minor modifications.[79] To count the number of c-Fos-positive cells in the mPFC-NAc or mPFC-VTA (Figures S1C–S1H), the subject mice were sacrificed 90 min after performing the last tube test. Coronal sections containing the mPFC were prepared for c-Fos immunostaining, and the viral injection sites were confirmed in sections containing the NAc and VTA. The mPFC sections were incubated in blocking solution (0.3% triton-X 100 and 4% normal donkey serum in PBS) for 1 h at room temperature and then incubated with rabbit anti-c-Fos antibody (1:2,000, 2250S, Cell signaling technology) overnight at 4°C. Following 3 × 10 min washing in PBS, incubation with donkey anti-rabbit Alexa Fluor 647 (1:200, A-31573, Invitrogen) was done for 3 h at room temperature. Sections were washed with PBS for 3 × 10 min, incubated in DAPI (1:5,000, 62248, Thermo Scientific) solution, and washed again. Stained sections were mounted on slides (Muto pure chemicals) and cover-slipped with VectaMount Permanent Mounting Medium (H-5000, Vector Laboratories). All

images were obtained using ultra high-speed & spectral confocal microscopy (A1 Rsi/Ti-E, Nikon, Japan) at equal gain and exposure with a 10X objective lens.

For quantification of the efficiency of *Pou3f1* knockdown or overexpression (Figures S9A, S9B, S9E, and S9F), coronal sections containing the mPFC were immunostained for Pou3f1 by incubating with rabbit anti-Pou3f1 antibody (1:500, ab272925, abcam) overnight at 4°C. The brain sections were then exposed to donkey anti-rabbit Alexa Fluor 555 antibody (1:500, A-31572, Invitrogen) for 2 hours. After washing and mounting on the slide slice, images were acquired using a fluorescence microscope (Pannoramic Scan system, 3DHISTECH) at the same gain and exposure with a 20X objective lens.

Immunostaining or FISH were not performed for Figures 1C, 1G, 2B, 3B, 3F, 3J, 3P, 7B, S1B, S4H, S4I, and S4Q.

For FISH experiments (Figures 4D–4I, 5E, 5F, 7H, 7I, S7C–S7L, S10D, and S10E), brain sections were processed according to the hybridization chain reaction (HCR) RNA-FISH protocol (Molecular Instruments). Brain sections mounted on slide glasses were fixed in 4% PFA for 15 min at 4°C, dehydrated in serial ethanol washes (50%, 70%, 100%, and 100%, 5 min each at room temperature), treated with 10 μg/ml of proteinase K solution in a humidified chamber for 10 min at 37°C, and washed in PBS. Slides were then pre-hybridized with probe hybridization buffer in a humidified chamber for 10 min at 37°C. After removing pre-hybridization solution, probe mixture was applied to each slide and incubated overnight in a humidified chamber at 37°C. The probes used in this study were as follows: *Nptx2*, *Ly6a*, *Nrip3*, *Pou3f1*, *Nrn1*, *Cnih3*, *Ankrd33b*, and *Mpv17* (concentration of all probes: 4 nM). Slides were then washed in a series of probe wash buffer and 5x SSCT mixtures (1:0, 3:1, 1:1, 1:3, and 0:1) for 15 min each, at 37°C. Slides were washed again in 5x SSCT for 5 min before applying amplification buffer to each slide and incubating in the humidified chamber for 30 min at room temperature. Amplifiers (*Nptx2*, B1-488; *Ly6a*, B2-647; *Nrip3*, B1-488; *Pou3f1*, B4-647; *Nrn1*, B1-488; *Cnih3*, B1-488; *Ankrd33b*, B3-546; *Mpv17*, B3-546; concentration of all amplifiers: 60 nM) were mixed with amplification buffer and it was applied to each slide and incubated overnight in a dark humidified chamber at room temperature. Finally, slides were washed in 5x SSCT and cover-slipped with mounting medium. Images were acquired using a confocal microscope (TCS SP8, Leica) with a 63X objective lens.

Fiber photometry

All fiber photometry experiments were conducted using Doric Fiber Photometry System (Doric Lenses). The two connectorized LEDs (CLEDs, 405 nm regulated at 208.616 Hz for calcium-independent signals and 465 nm regulated at 572.205 Hz for calcium-dependent signals) were controlled by the fiber photometry console via the LED driver. Each CLED was coupled to Integrated Fluorescence Mini Cube with 4 ports (iIFMC4_IE(400-410)_E(460-490)-F(500-550)_S) via an attenuating patch cord, and S port of the Mini Cube was coupled to a mono fiber-optic patchcord to deliver the excitation light to and to receive emitted light from behaving mice. The F(500-550) port of the Mini Cube was coupled to the photodetector (Fluorescence Detector Amplifier, Doric Lenses) that was coupled to an analog port of the fiber photometry console. Fiber photometry signals were recorded by Doric Neuroscience Studio (Ver. 5.3.3.14) through the Lock-In mode and a sampling rate of 12.0 kS/s. All recorded signals were decimated by a factor of 12. Tube tests with fiber photometry were recorded by a behavior tracking camera (Doric Lenses) controlled by the same software to synchronize the tube test behaviors and the recorded neural activities.

Ex vivo electrophysiology

All electrophysiological experiments were conducted 1 day after the final tube test, and brain slices from R1 and R4 mice were prepared at the same time to minimize the change in conditions due to the time difference when the two mice were sacrificed separately. Electrophysiological recordings were performed as we previously described with minor modifications.[80–82] Briefly, mice were anesthetized with isoflurane. After decapitation, the brains were removed rapidly and then submerged in an ice-cold, oxygenated (95% O_2 and 5% CO_2), low-Ca^{2+} / high-Mg^{2+} dissection buffer containing 2.5 mM KCl, 1.23 mM NaH_2PO_4, 26 mM $NaHCO_3$, 11 mM dextrose, 0.5 mM $CaCl_2$, 10 mM $MgCl_2$, and 212.7 mM Sucrose. Coronal brain slices (300 μm) containing the mPFC and NAc or VTA (to check injection sites of retrograde viruses) were cut using a vibratome (VT1200S, Leica Biosystems). After that, the brain slices were put in a recovery chamber filled with oxygenated artificial cerebrospinal fluid (ACSF), which contained 124 mM NaCl, 2.5 mM KCl, 1.23 mM NaH_2PO_4, 26 mM $NaHCO_3$, 11 mM dextrose, 2.0 mM $CaCl_2$, and 1.0 mM $MgCl_2$, and incubated at room temperature (24-26°C) for at least an hour before recording.

After recovery, the slices were moved to a submerged recording chamber where they were continuously perfused with oxygenated ACSF that was kept at room temperature at a flow rate of 2 ml/min. Slices were stabilized for at least 5 min prior to the recordings, and then whole-cell patch clamp recordings on retrogradely labeled mPFC pyramidal neurons were made using borosilicate glass pipettes (4-6 MΩ) filled with the internal solution containing 123 mM K-gluconate, 12 mM KCl, 10 mM HEPES, 0.2 mM EGTA, 4 mM Mg-ATP, 0.3 mM Na-GTP, and 10 mM Na_2-phosphocreatine at pH 7.2-7.4 and 280-290 mOsm. Neuronal intrinsic properties such as excitability (Figures S2A, S2B, S2H, and S2I), rheobase current measurement (Figures S2C, S2D, S2J, and S2K), membrane capacitance (Cm) (Figures S2E and S2L), resting input resistance (R_{In}) (Figures S2F and S2M), and resting membrane potential (RMP) (Figures S2G and S2N) were recorded under the current clamp mode. Only cells having an input resistance of more than 100 MΩ and an access resistance of less than 20 MΩ were recorded. The cells were excluded if the input or access resistance changed by more than 20%. Signals were amplified by a Multiclamp 700B (Molecular devices) and filtered at 2 kHz and digitized at 10 kHz with Digidata 1550B (Molecular Devices). Data were recorded and analyzed using pClamp 10 (Molecular Devices).

Please cite this article in press as: Choi et al., Distinct prefrontal projection activity and transcriptional state conversely orchestrate social competition and hierarchy, Neuron (2023), https://doi.org/10.1016/j.neuron.2023.11.012

Tissue collection and library preparation for single-cell RNA sequencing

Animals were anesthetized with CO_2 and the brains were extracted and transferred into ice-cold Dulbecco's phosphate-buffered saline (DPBS) one day after the last tube test. For single cell dissociation, the brains were sectioned into 1.0 mm coronal slices in ice-cold DPBS with the brain matrix, and the mPFC was collected from each slice using 14-gauge punches (BP-10F, Kai Medical). In total, five pooled independent biological replicates including tissues from two-to-three different mice were analyzed for sequencing. Briefly, the tissues were cut into small pieces and incubated in a dissociation media (Hibernate A without Calcium and Magnesium with 1 mg/ml papain, 50% D-(+)-trehalose dihydrate, 25 mM DL-2-amino-5-phosphonopentanoic acid and DNase I) at 37°C for 60 min with shaking at 225 RPM. After washing with 5 ml Hibernate A medium, the tissues were mechanically triturated with cutting pipette tips (tip diameter 2 mm and 1 mm) in 2 ml Hibernate A medium, which was repeated for another two times, and filtered through a cell strainer with 70 μm of the pore size to release single cells. The 1.5 ml single-cell suspension was pooled and loaded on a gradient medium (Hibernate A without Calcium and Magnesium with 1 mg/ml papain, 50% D-(+)-trehalose dehydrate, 25 mM DL-2-amino-5-phosphonopentanoic acid, DNase I, and ovomucoid inhibitor-albumin) and centrifuged at 900 RPM for 6 min at 4°C to remove debris. The cells were then washed with 1 ml Hibernate A medium followed by 1 ml DPBS. The cells were spun down at 1,250 RPM for 6 min and re-suspended in DPBS. Countess II Automated Cell Counter (Invitrogen) was used to count the number of cells after centrifugation.1,000 ∼ 1,800 cells/μl or 1,500 ∼ 3,200 cells/μl were obtained from samples from two or three pooled mice, respectively.

For single cell RNA-sequencing (scRNA-seq), the cell suspension was diluted to the recommended concentration (700 ∼ 1,200 cells/μl) of the manufacturer's protocol. We prepared cell suspension to 10,000 targeted cell recovery, and it was captured with 10X Chromium platform (10X Genomics, CA). 10x Genomics Chromium platform delivers a microfluidic chip for 3' digital gene expression by profiling 500-10,000 individual cells per sample. Using Chromium Single Cell 3' Reagent Kits v3, we prepared single cell master mix and gel beads, and then generated Gel Beads-in-emulsion (GEMs), combining barcoded Single Cell 3' v3 Gel Beads. Next, the Gel Beads were dissolved, and cDNA was synthesized according to the sequence included in the GEMs. Since cDNA was synthesized, GEMs were broken and silane magnetic beads were used to purify the first-strand cDNA. And then, cDNA was amplified to generate sufficient mass for library for sequencing. Libraries were generated and sequenced from the cDNA and 10x Barcode containing the GEMs. The final libraries contained the P5 and P7 primers used in Illumina bridge amplification and the concentration was 1.7∼2.7μg.

Single-cell real-time quantitative PCR

Single cell RT-qPCR (scRT-qPCR) was carried out as previously described with minor modification.[83–86] RNA was isolated from retrogradely labeled mPFC-NAc or mPFC-VTA neurons from the coronal brain section containing mPFC 1 day after the final tube test. All glassware was oven-baked at 180°C for at least 12 h, and all buffers and solutions were prepared using nuclease-free water (AM9932, Invitrogen) to minimize RNase contamination. Preparation of brain slices and whole-cell patch clamp recordings were performed as described in the *Ex vivo* electrophysiology section. Cells were aspirated with borosilicate glass pipettes (4-6 MΩ) filled with the same internal solution for electrophysiological recordings added 20 μg/ml glycogen and RNase inhibitor (0.16 Units/μL; SUPERaseIn RNase inhibitor (20 U/μL); AM2694, Invitrogen). After making a whole-cell configuration, intracellular contents including the nucleus were gently aspirated by applying negative pressure,[78] and the shape and the holding current of aspirated neurons were monitored to check the quality of the aspiration. RNA extraction from collected intracellular contents and reverse transcription were performed using a Sing Cell-to-CT™ qRT-PCR kit (4458237, Invitrogen). In the pre-amplification and real-time PCR procedures, Taqman gene expression assays (*Nptx2*, Mm00479438_m1; *Nrn1*, Mm00467844_m1; *Cnih3*, Mm01319298_m1; *Ankrd33b*, Mm07298789_m1; *Mpv17*, Mm00485133_m1; *Nrip3*, Mm00508049_m1; *Pou3f1*, Mm00843534_s1; *Ly6a*, Mm00726565_s1; *Rn18s*, Mm03928990_g1; Thermo Fisher Scientific) were used. Amplification of cDNA was performed using LightCycler 480 Instrument II (Roche, Swiss), and then all reactions were analyzed using ΔΔCt method as previously described[87] with 18S ribosomal RNA (*Rn18S*) as a normalized control.

QUANTIFICATION AND STATISTICAL ANALYSIS

Quantification of FosTRAPed neurons and projections

The number of tdTomato-expressing neurons in the mPFC (mainly prelimbic (PrL) or dorsomedial prefrontal cortex (dmPFC) located in A.P. +2.3 ∼ +1.9) was manually counted in the region of interest (ROI, 581.25 x 581.25 μm). Animals with infected cells in areas outside of these specific coordinates, such as the infralimbic (IL) or secondary motor cortex (M2), were excluded from the analysis. Puncta density in the ROI (184.52 x 184.52 μm) was measured as instructed with minor modifications.[88,89] The density of synaptic puncta which express SypEGFP was quantified in ImageJ using the 3D Objects Counter plug-in. Threshold values were set for each ROI to subtract background fluorescence. Volumetric puncta density was calculated as puncta count/tissue volume (mm^3). Cell numbers and puncta density were averaged from eight sections per mouse. Measurements were normalized to the average of the control of each brain region. All procedures were done by a blinder observer.

Quantification of TRACE-labeled or c-Fos-positive cells

The number of TRACE-labeled or c-Fos-positive cells in the ROI (500 × 500 μm) was counted by ImageJ by a blinder observer. Cell numbers of eight coronal sections per mouse were averaged.

Fiber photometry analysis

Data analysis was conducted using an open-source analysis package, named photometry modular analysis (pMAT).[74] The onsets of each behavior were synchronized to time zero, and Z-score standardization was applied to the signals. The averaged response to each tube test behavior was calculated by subtracting the average Z-scored data 1 s prior to and 2 s after the behavioral onset. Trials that include other social competition behaviors during the analysis period – 1 s prior to and 2 s after behavioral onset of specific behavior – were excluded from the final analysis. The area under the curve (AUC) per second values were calculated to compare the neural activity before and after the behavioral onset of each animal.

scRNA-seq data processing, clustering, and annotation

Raw sequencing data from 10 samples, five biological replicates for each rank, were quantified using 10x Genomics Cell Ranger 4.0.0.[75] Mouse mm10 reference recommended and provided by 10x Genomics (Pleasanton, CA) was used. Then, Seurat package 3.1.3 in R was used for subsequent data processing.[76] As a quality control, cells that expressed too few or too many genes were excluded (Table S1). In addition, cells with high expression rates of mitochondrial, ribosomal, and hemoglobin genes were considered low-quality and excluded. Details on filtering criteria and the number of cells generated from each sample are in Table S1. Then, Log Normalization and data integration to correct batch effect were conducted using Seurat. For clustering, the first 20 principal components were used to create k-nearest neighbor (KNN) graphs and Uniform Manifold Approximation and Projection (UMAP) and FindClusters function, implementing the Louvain algorithm, in Seurat with the resolution of 0.2 was used. Cell type annotation was performed using the SingleR package.[90] In-house cluster reference gene lists were used for annotation. Multiple test corrections were applied where needed and the P-values were adjusted by the FindMarkers function of Seurat, which uses Bonferroni correction.

mPFC-NAc or mPFC-VTA classification and DEG analysis

Neuronal cells were isolated and subjected to PCA, UMAP, and clustering based on the expression of enriched genes of NAc- or VTA-projecting mPFC neurons in the previously reported study[26] using the same parameter. Seurat's FindMarkers function was used to find the marker gene for each cluster with logfc.threshold parameter of 0.25, the test method of the Wilcoxon Rank Sum test. Genes with p-adj < 0.05 was defined as cluster marker genes. Then, DEGs were found between R1 and R4 using the FindMarkers function with the same parameters.

Pou3f1 chromatin immunoprecipitation sequencing data analysis

We downloaded Pou3f1 chromatin immunoprecipitation sequencing (ChIP-seq) peak bed files from previous studies (corresponding GEO: GSE110950, GSE74636, GSE54569, and GSE69778). ChIPseeker package 1.32.1 was used to annotate peak. Transcription start site regions were defined as ± 3 kb of transcription start sites. TxDb.Mmusculus.UCSC.mm9.knownGene R package was used as an annotation database. Gene ontology (GO) enrichment analysis was conducted using clusterProfiler package 4.4.4 with multiple test-adjusted p value threshold of 0.05.

scRT-qPCR and clustering

Calculated Ct values were used in clustering methods. The value of ΔCt was the calculated result of (Ct value of target gene – Ct value of Rn18s gene), and the value of ΔΔCt was the calculated results of (each ΔCt / average of ΔCt of R1 group). Finally, the fold change values (2-ΔΔCT) of cluster markers (C8, Ly6a; C0, Nrip3) were used to cluster C1 or C8 from mPFC-NAc neurons and C0 or C3 from mPFC-VTA neurons. The Expectation-Maximization (EM) or Simple K-means analysis in Machine Learning Algorithm in JAVA (WEKA, New Zealand) system was used for the clustering of the scRT-qPCR data. The relative values of mRNA fold change were classified according to the clustering result.

FISH

FISH images were analyzed using methods described in previous studies.[27,62,91] The expression of cluster marker genes and DEGs of FISH images was identified by visual inspection of each confocal image. Clusters were determined by the presence or absence of cluster-specific marker genes – C1, *Nptx2*; C8, *Ly6a*; C0, *Nrip3*; C3, *Pou3f1* - in retrogradely labeled neurons. To quantify the number of puncta of DEG candidates, *Pou31*, *Nptx2*, *Nrn1*, *Cnih3*, *Ankrd33b*, and *Mpv17*, the number of puncta of each gene localized in retrogradely labeled individual cells were analyzed. FISH signals of DEG candidates were selected with a fixed threshold of intensity and size using multi-particle analysis.

Statistical analysis

The number of biological replicates was reported, and several internal replications are present in the study. Animals were randomly assigned to treatment groups. Every experiment used anonymous samples, and the experimenters were not informed of the experimental conditions of the animals. No data were excluded after analyses.

Statistical analyses were conducted using GraphPad Prism 9 or 10. For n sizes, the number of animals or cells were provided in Figure legends. Data are presented as mean ± the standard error of the mean (SEM) or individual plots. Effect size was estimated using partial eta squared (η_p^2). Comprehensive information on statistical analysis is included in the figure legends and Table S4.